Modes of Interannual Tropical Ocean–Atmosphere Interaction—a Unified View. Part I: Numerical Results

FEI-FEI JIN* AND J. DAVID NEELIN

Department of Atmospheric Sciences, University of California, Los Angeles, Los Angeles, California

(Manuscript received 6 October 1992, in final form 1 February 1993)

ABSTRACT

Coupled ocean–atmosphere models exhibit a variety of forms of tropical interannual variability that may be understood as different flow regimes of the coupled system. The parameter dependence of the primary bifurcation is examined in a "stripped-down" version of the Zebiak and Cane model using the equatorial band approximation for the sea surface temperature (SST) equation as by Neelin. In Part I of this three-part series, numerical results are obtained for a conventional semispectral version; Parts II and III use an integral formulation to generate analytical results in simplifying limits. In the uncoupled case and in the fast-wave limit (where oceanic adjustment occurs fast compared to SST time scales), distinct sets of modes occur that are primarily related to the time scales of SST change (SST modes) and of oceanic adjustment (ocean-dynamics modes). Elsewhere in the parameter space, the leading modes are best characterized as *mixed SST/ocean-dynamics modes;* in particular, the continuous surfaces in parameter space formed by the eigenvalues of each type of mode can join.

A regime in the fast-wave limit in which the most unstable mode is purely growing, with SST anomalies in the eastern Pacific, proves to be a useful starting point for describing these mergers. This mode is linked to several oscillatory regimes by surfaces of degeneracy in the parameter space, at which two degrees of freedom merge. Within the fast-wave limit, changes in parameters controlling the strength of the surface layer or the atmospheric structure produce continuous transition of the stationary mode to propagating modes. Away from the fast-wave limit, the stationary mode persists at strong coupling even when time scales of ocean dynamics become important. On the weaker coupling side, the stationary mode joins to an oscillatory mode with mixed properties, with a standing oscillation in SST whose growth and spatial form may be understood from the SST mode at the fast-wave limit but whose period depends on subsurface oceanic dynamics. The oceanic dynamics, however, is only remotely related to that of the uncoupled problem. In fact, this standing-oscillatory mixed mode is insensitive to low-coupling complications involving connections to a sequence of uncoupled ocean modes at different parameter values, most of which are members of a discretized scattering spectrum. The implication that realistic coupled regimes are best understood from strong rather than weak coupling is pursued in Parts II and III. The interpretation of the standing-oscillatory regime as a stationary SST mode perturbed by wave dynamics gives a rigorous basis to the original physical interpretation of a simple model of Suarez and Schopf. However, viewing the connected modes as different regimes of a mixed SST/ocean-dynamics mode allows other simple models to be interpreted as alternate approximations to the same eigensurface; it also makes clear why varying degrees of propagating and standing oscillation can coexist in the same coupled mode.

1. Introduction

The importance of tropical ocean–atmosphere interaction has been recognized since Bjerknes (1969) first hypothesized its role in the El Niño–Southern Oscillation (ENSO) phenomenon, the most prominent interannual oscillation of the tropical climate system. The essence of Bjerknes' postulate still stands as the basis of present-day work—that ENSO arises as a self-sustained cycle in which anomalies of sea surface temperature (SST) in the Pacific cause the trade winds to strengthen or slacken, and that this in turn drives the ocean circulation changes that produce anomalous SST. Beginning at about the same time, the foundations for modeling the tropical coupled system were laid through the study of the individual components: the dynamics of the equatorial ocean response to wind stress in shallow-water models (e.g., Moore 1968; Cane and Sarachik 1977, 1981; McCreary 1976), modified shallow-water models (e.g., Cane 1979a,b; Schopf and Cane 1983) and ocean general circulation models (ocean GCMs or OGCMs; e.g., Philander and Pacanowski 1980; Philander 1981); and the semiempirical finding that simple atmospheric models with steady, damped shallow-water dynamics could provide a reasonable approximation to the low-level tropical atmospheric response to SST anomalies (e.g., Matsuno 1966; Gill 1980; Gill and Rasmusson 1983).

* Current affiliation: Department of Meteorology, University of Hawaii at Manoa, Honolulu, Hawaii.

Corresponding author address: Prof. J. David Neelin, Dept. of Atmospheric Sciences, UCLA, 405 Hilgard Ave., Los Angeles, CA 90024-1565.

The basis for a more quantitative understanding of coupled ocean–atmosphere interaction was provided by coupled models constructed from variations on such modified shallow-water ocean and simple atmospheric models: both in simple linear versions (Lau 1981; Philander et al. 1984; Gill 1985; Hirst 1986, 1988; Wakata and Sarachik 1991; Neelin 1991) and nonlinear versions (e.g., Cane and Zebiak 1985; Anderson and McCreary 1985; Zebiak and Cane 1987; Battisti 1988; Battisti and Hirst 1989; Schopf and Suarez 1988; Yamagata and Masumoto 1989; Graham and White 1990). The latter are often referred to as "intermediate" coupled models within a model hierarchy that now also includes, in order of increasing complexity, hybrid coupled models (consisting of an ocean GCM coupled to a simpler atmospheric model, e.g., Neelin 1989b, 1990; Latif and Villwock 1990; Barnett et al. 1993, personal communication) and coupled GCMs (in which both components include relatively complete physical parameterizations and primitive equation dynamics, e.g., Philander et al. 1989; Philander et al. 1992; Lau et al. 1992; Sperber and Hameed 1991; Gordon 1989; Meehl 1990; Nagai et al. 1992; Mechoso et al. 1993; Neelin et al. 1992). Most of these models produce interannual variability through coupled interactions that have significant parallels to ENSO dynamics.

However, there are very considerable differences in the nature of the coupled variability produced by the different models (e.g., Neelin et al. 1992). In models where parameter dependence has been examined, the system shows considerable sensitivity and a rich variety of flow regimes have been found, both in nonlinear systems (e.g., Zebiak and Cane 1987, hereafter ZC; Battisti 1988; Neelin 1990; Ghil et al. 1991) and in linear models that exhibit multiple mechanisms of coupled interaction (e.g., Hirst 1986, 1988; Battisti and Hirst 1989; Neelin 1991, hereafter N91; Wakata and Sarachik 1991). The character of the interannual variability in nonlinear models is largely determined by the first bifurcation from the climate state (Neelin 1990; Münnich et al. 1991); in other words, by the leading unstable mode of the system linearized about the climatological state. Many of the most pressing questions about the range of coupled variability found in coupled models can thus be addressed by understanding the relation between flow regimes in the linear problem.

At the same time, the search for simple prototype systems to provide conceptual analogs for the modes of coupled variability has led in a number of apparently contradictory directions. Much current terminology is based on the Rossby and Kelvin modes of the uncoupled ocean in an infinite or periodic basin, presumably because these are most familiar to oceanographers. A significant step toward thinking in terms of the fully coupled problem was advanced by Schopf and Suarez (1988) and Suarez and Schopf (1988, SS hereafter) using a "toy" model with a single spatial variable to explain the oscillation in their intermediate coupled model; Battisti and Hirst (1989, BH hereafter) showed that a version of this model could be fit to a number of important aspects of the oscillation in the ZC model. Often referred to as the delayed-oscillator model, it consists of a differential-delay equation representing the time evolution of SST averaged over a small eastern equatorial box, with a net growth tendency representing local positive feedback mechanisms due to coupling and a delayed negative feedback representing the equatorial wave adjustment process; how literally the latter should be interpreted in terms of off-equatorial Rossby wave packets reflecting from the western boundary has been the subject of debate (Graham and White 1988; Battisti 1989). The model is designed to represent the regime in which SST variability occurs as a standing oscillation in the strongly coupled eastern basin, and in which time scales of ocean wave dynamics provide the "memory" of the system essential to the oscillation.

On the other hand, a large class of coupled regimes exists in which the time scales of ocean wave dynamics are not essential to interannual oscillation. A distorted physics method for testing this was employed in N91 to show that artificial increases to the wave speed in the OGCM component of a hybrid coupled model did not fundamentally affect the oscillation in a moderate-coupling flow regime. An idealized but mathematically and conceptually useful limit was introduced to explain oscillations of this type: in the fast-wave limit, the time scales of dynamical adjustment of the ocean are taken to be fast compared to the time scales of SST evolution through coupled processes. The slow modes of the coupled system are then associated with the time derivative of the SST equation, and hence referred to as SST modes. Steady-state ocean dynamics is crucial to SST modes in the fast-wave limit, but wave time scales, by definition, are not. Hirst (1986, 1988) and N91 showed, by numerical and analytical methods, respectively, that a number of physical processes cooperate in the destabilization of SST modes, whereas they compete in terms of the direction of propagation. Propagation is essential to the period in these modes and they provide a good prototype for slowly propagating modes in a number of intermediate models and GCMs (e.g., Anderson and McCreary 1985; Yamagata and Masumoto 1989; Meehl 1990; Lau et al. 1992).

Because the SS delayed oscillator model is based on the SST equation, it was natural to hypothesize that nonpropagating SST modes away from the fast-wave limit might be perturbed by wave time scales to produce standing oscillations. Such a connection is inherent in Wakata and Sarachik (1991) in which the relation between a propagating regime of Hirst (1988) and a standing-oscillation regime is demonstrated. Puzzlingly, two models aimed at producing more rigorous derivations of the SS delayed oscillator, Cane et al. (1990, CMZ hereafter) and Schopf and Suarez (1990), are formulated in what we call the fast-SST limit: the

limit in which time scales of SST adjustment are assumed to occur fast compared to time scales of ocean wave dynamics, that is, the converse of the fast-wave limit. These models are also constrained to assume the coupling occurs at a single point rather than across all or most of the basin.

It is our purpose in this three-part paper to show how such seemingly contrary idealizations of a coupled mode can be reconciled, to make connections between different flow regimes for the leading coupled modes in a finite basin, and to provide prototypes for coupled mode behavior in system where partial differential equations for spatial structure are solved explicitly. We use two versions of the "stripped-down" intermediate model introduced in N91 and here solved in a finite basin. The model is designed to capture all the essential mechanisms of the ZC model, but with simplifications that permit more detailed analysis. In Part I, we approach the problem numerically using a conventional semispectral method for the ocean component. In Part II, a formulation of the model is derived that permits analytical or near-analytical solutions to be derived in special limits; the low-coupling limit is outlined in Part II, while the more novel fully coupled cases are elaborated in Part III.

To keep this multiparameter bifurcation problem tractable, the key is to choose a few crucial parameters that capture the range of behavior of interest, and to restrict the exploration to regimes that are either close to that of the real system or provide useful simplifications while remaining closely connected to the realistic regimes. A detailed scaling to justify the parameters chosen is given in Part II with the analytic model derivation and a discussion of the ranges of validity of the several limits employed; in Part I the parameters are introduced on a more pragmatic basis. The tracing of modes—temporal eigenvalues and the corresponding spatial structures—through parameter space is emphasized in both numerical and analytical work. It proves simpler in terms of articulating the physical relation between modes in different regimes to trace the few leading modes (i.e., most unstable or least stable) rather than restricting attention to where the leading mode first becomes unstable. Obviously, the leading mode is directly related to a primary bifurcation of the original system whenever it is destabilized relative to the explicit damping.

Surfaces of continuously connected eigenvalues (eigensurfaces hereafter) corresponding to different modes remain distinct through subregions of parameter space, but singularities occur at which two or more eigensurfaces join. A large literature of techniques for exploiting such singularities exists (e.g., Golubitsky and Schaeffer 1985; Golubitsky et al. 1988); we confine attention to the properties that provide insight into how coupled modes are constructed. It proves convenient here to refer to these by the algebraic multiplicity of the degenerate eigenvalues and corresponding eigenvectors: for example, 2-degeneracy for the degeneracy of multiplicity two that occurs when a pair of eigenvalues merges. Some, but not all, of these degeneracies correspond to codimension two and higher bifurcations of the original system. A summary of some relevant properties is given for reference in the Appendix. While the degeneracies subdivide the parameter space in some respects, many physical properties of the modes are continuous across the degeneracies; other properties change without explicitly crossing a degeneracy. Discussion emphasizes the physical properties wherever possible, and in most cases this yields a good sense of why a degeneracy must occur, given the dominant balances in two regions.

In Part I, section 2 presents the model in conventional form with realistic basic state; section 3 outlines the connection between flow regimes within the fast-wave limit for this case to provide comparison to the analytical versions in Part III and to the more realistic parameter regimes of sections 4 and 5. Section 4 contains the heart of the paper: a detailed analysis of the connection between a regime with a purely growing SST mode in the fast-wave limit and the regimes where this mode becomes mixed with ocean-dynamical time scales. Section 5 examines some of the simplest nonlinear cases and section 6 provides conclusions for Part I, drawing also on results from Parts II and III.

2. Model

a. Ocean component

Among the intermediate coupled models, the ZC model has had considerable success at quantitative simulation of ENSO anomalies and even at prediction (Cane et al. 1986; Barnett et al. 1988). This results from a careful parameterization of the processes that affect SST and to the inclusion of an embedded surface layer for surface currents and equatorial upwelling due to Ekman-like dynamics, narrow equatorial upwelling being particularly crucial to the coupled problem. The ocean model component is closely related to that of ZC, but stripped down as in N91 to facilitate analysis. The principal simplification is motivated by the fact that the strongest surface temperature response to upwelling, advection, and thermocline depth changes is confined to a fairly narrow band along the equator in the ENSO phenomenon. Thus, a simple equation for SST in the equatorial band is constructed following N91. This equation governs the thermodynamics of a box of the surface mixed layer centered on the equator. With an upstream advection scheme for the vertical and meridional differencing of advection into the equatorial surface band, the total SST equation can be written as

$$\partial_t T + u_1 \partial_x T + \mathscr{H}(w)\frac{w}{H_{1.5}}(T - T_{\text{sub}}) - \mathscr{H}(-v_N)\frac{2v_N}{L_y}(T - T_N) + \epsilon_T(T - T_0) = 0, \quad (1)$$

where T is the surface mixed-layer temperature of the equatorial band, u_1 the zonal surface current, w and v_N the vertical and meridional surface currents appropriate for the upstream differencing, and $\mathscr{H}$ is an analytic version of the Heaviside function. The Newtonian cooling represents all physical processes that bring the system toward a radiative–convective–mixing equilibrium in absence of dynamical advection with $T_0 = 29°C$ the equilibrium SST value at the equator; L_y is the width of the box, T_N is the off-equatorial SST at a distance L_y from the equator, and $H_{1.5} = 75$ m is the depth scale characterizing upwelling of subsurface temperatures, T_{sub}, from the underlying shallow-water layer. Here we set $T_N = T_0$ and assume symmetry of SST and antisymmetry of the meridional current. A diffusion term can be useful when considering certain aspects of very weakly coupled cases (see Part II) but makes no difference to the numerical results considered here.

A parameterization like that of Zebiak and Cane (1987) is employed for the effect of the vertical displacement of the thermocline on the subsurface temperature,

$$T_{\text{sub}} = T_{s0} + (T_0 - T_{s0}) \tanh[(h_e + h_0)/H^*]. \quad (2)$$

Here T_{s0} is the characteristic temperature being upwelled into the surface layer and h_e is the equatorial value of the thermocline depth departure from its no-motion value. This formulation guarantees that T_{sub} is between T_0 and $T_{s0} - 2(T_0 - T_{s0})$, providing bounding nonlinearity in the thermocline feedback. Here T_{s0} is the temperature at an offset $-h_0$ from the thermocline, say the 20°C isotherm, where h_0 and H^* control the asymmetry of the thermocline depth dependence and the maximum rate of change, respectively. Positive h_0 is appropriate, because it results in a greater dependence of T_{sub} on h where the thermocline is relatively shallow; $H^* = 25$ m, $h_0 = 30$ m are chosen to give reasonable sensitivity of temperature to thermocline depth anomaly in the eastern part of the basin. This simple parameterization may not give as good a fit for interannual variability as the Zebiak and Cane (1987) parameterization from which it was inspired. However, the analytic dependence ensures nice properties for the system and we are concerned with qualitative properties rather than the exact amplitude of anomalies.

Following N91, v_N is obtained by finite differencing of the continuity equation:

$$2\frac{v_N}{Ly} = \frac{w}{H_1} - \frac{\partial u_1}{\partial x}. \quad (3)$$

Thus, the equatorial SST change involves only the equatorial values of u_1, w, and h. The ocean-dynamics component consists of a modified shallow-water model with an embedded, fixed-depth mixed layer, following ZC. With subscript 1 for the surface mixed layer and 2 for the underlying shallow water layer, the equations can be written as

$$\epsilon_s u_s - \beta y v_s = \frac{\tau H_2}{\rho H_1 H}$$

$$\epsilon_s v_s + \beta y u_s = 0 \quad (4)$$

and

$$\delta\partial_t u_m + \epsilon_m u_m - \beta y v_m + g\partial_x h = \frac{\tau}{\rho H}$$

$$\beta y u_m + g\partial_y h = 0$$

$$\delta\partial_t h + \epsilon_m h + H(\partial_x u_m + \partial_y v_m) = 0, \quad (5)$$

where

$$u_m = (H_1 u_1 + H_2 u_2)/H, \quad u_s = (u_1 - u_2)H_2/H$$

$$u_1 = u_s + u_m, \quad w = w_s + w_m, \quad H = H_1 + H_2; \quad (6)$$

H_1 and H_2 are the mean height of the two layers, set to 50 m and 100 m, respectively, and ρ is the oceanic density. The reduced gravity parameter, g, is chosen to give a Kelvin wave speed $c_0^2 = gH$, about 2.7 m s^{-1}. In Eqs. (4) and (5), the meridional component of the wind stress is neglected because the wind perturbations are predominantly zonal in the phenomenon of interest and meridional wind stress has a smaller effect at large zonal scales in the ocean. Advective nonlinearity in the shallow-water component is neglected since the applicability of shallow-water dynamics to the three-dimensional ocean would fail before such terms could be important. The small effects of SST on the dynamics component through density changes are neglected, as in ZC.

To get magnitudes of w_s and u_s comparable with the observations, a strong damping coefficient is required for the transfer of momentum between the surface layer and the remainder of the shallow water layer, $\epsilon_s = (2 \text{ days})^{-1}$, while for the two-layer vertical-mean motion a weak damping rate $\epsilon_m = (2.5 \text{ yr})^{-1}$ is used. Equations (4) are readily solved for the equatorial values of u_s and w_s. Equations (5) are solved by conventional methods for time-dependent equatorial wave dynamics and u_m, w_m, and h are evaluated at the equator for use in the SST equation. The usual boundary conditions for the shallow-water equations in the long-wave approximation are used:

$$u_m(x = x_E, y) = 0, \quad \int_{-\infty}^{\infty} u_m(x = x_W, y)dy = 0. \quad (7)$$

The wave equations are expanded in parabolic-cylinder functions following Gill and Clark (1974). We use a standard truncation that includes the Kelvin mode and the first seven symmetric Rossby modes, with finite differencing of the first-order wave equations in the x direction on a 3-degree grid (48 points). This resolution was verified to be sufficient for convergence of results for the model basic state and leading coupled eigenmodes over most of the parameter domain; the discre-

tized scattering spectrum at low coupling is always resolution dependent.

A useful free parameter, δ, is introduced in (5) for the purpose of discussing the importance of the oceanic wave dynamics. As it appears here, it is similar to the distorted physics experiments of N91; in Part II it is motivated by more general scaling arguments. It measures the ratio of the time scale of adjustment by oceanic dynamics to the net time scale of SST change through various feedbacks acting through the SST equation. An important special case of the model arises when this ratio is small, and the fast-wave limit of N91 can be used. By dropping the time derivatives in (5), that is, $\delta = 0$, and considering the fact that ϵ_m is a very weak damping, the shallow-water equations reduce to Sverdrup balance along the equator,

$$g\partial_x h = \frac{\tau}{\rho H} \tag{8}$$

with negligible vertical mean currents. A proper boundary condition is required for (8), as discussed in Part III and in Hao et al. (1992, hereafter HNJ), both of which provide more detailed analysis of this fast-wave limit case.

b. *Atmospheric component*

In the dynamics of the tropical lower troposphere, mechanical balances are between pressure gradient, Coriolis force, and boundary-layer friction, while the thermodynamical balances are between diabatic heating and divergent flow acting in both moisture convergence and adiabatic cooling to a zeroth-order approximation. Although simple models based on these balances differ in physical interpretation (Lindzen and Nigam 1987; Neelin 1988; Neelin and Held 1987; Zebiak 1986), all approximately give an equivalent Gill-type model (Gill 1980) through proper scaling (Neelin 1989a). Thus, we follow the equations of Gill on an equatorial β plane,

$$\epsilon_a^* u_a - \beta y v_a + \partial_x \phi_a = 0$$

$$\beta y u_a + \partial_y \phi_a = 0$$

$$\epsilon_a^* \phi_a + C_a^2(\partial_x u_a + \partial_y v_a) = -Q, \tag{9}$$

where ϵ_a^* is the inverse time scale of boundary-layer friction and u_a, v_a, ϕ_a are boundary-layer winds and geopotential; C_a has the dimensions of gravity wave speed, and Q is a forcing term proportional to SST perturbation. In Gill (1980), Q was interpreted as a diabatic heating, and C_a^2 as a dry gravity wave speed; in more recent models, C_a^2 is reinterpreted and the bulk of the diabatic heating is associated with the convergence term.

In this coupled model, the SST meridional structure is fixed and hence that of Q. Hao et al. find little sensitivity to this structure so, for simplicity, we adopt

$$Q = A_0^* T'(x) \exp(-y^2/2L_a^2), \tag{10}$$

where $L_a = (C_a/\beta)^{1/2}$ is the atmospheric Rossby radius and T' is the SST anomaly. In this case, only the Kelvin mode and first Rossby mode are included in the response to the SST anomaly. Inclusion of more Rossby modes for other meridional structures does not substantially affect the relation of equatorial SST anomaly and wind stress. The wind stress on the surface of the ocean is $\tau' = \epsilon_a^* \rho_a H_a u_a$, consistent with the friction force on the atmosphere, where ρ_a, H_a are the atmospheric boundary-layer density and height. The wind stress along the equator is thus

$$\tau'(x) = \mu A\Big(\frac{3}{2}\exp(3\epsilon_a x/L) \times \int_x^{x_E} T'(x)\exp(-3\epsilon_a x/L)dx/L - \frac{1}{2}\exp(-\epsilon_a x/L)\int_{x_W}^{x} T'(x)\exp(\epsilon_a x/L)dx/L\Big) \tag{11a}$$

$$A \equiv A_0\epsilon_a = (\rho_a H_a/C_a)A_0^*\epsilon_a, \tag{11b}$$

where $\epsilon_a = \epsilon_a^* C_a^{-1} L$ is the inverse spatial damping scale of the atmospheric response, nondimensionalized by the ocean basin width, L. A typical value for reasonable atmospheric damping is $\epsilon_a \approx 2.5$. Considering that for this ϵ_a, a constant 1°C SST anomaly over one-third of the basin yields maximum westerly stress of $\mu A/5$, $A = 0.05$ (Pa K^{-1}) is a reasonable value (on the moderately strong end of the coupling range) for the wind stress response to SST anomalies estimated from observations. Thus, we take $A_0 = 0.02$ Pa K^{-1} as a standard value. The relative coupling coefficient μ is a free scalar parameter used to go between uncoupled and strongly coupled cases.

In the Lindzen–Nigam interpretation, in which $A = (\epsilon_c\epsilon_a^*)^{1/2}(gH_a)^{1/2}\rho_a H_a(2T_a)^{-1}$, where T_a is the surface temperature, $C_a^2 = (\epsilon_a^*/\epsilon_c)gH_a$, and ϵ_c is a "cumulus adjustment time" of around 30 minutes, similar values are obtained.

c. *Basic state and coupling*

To produce a reasonably realistic basic state for the model, while maintaining consistency between the ocean dynamics in the basic state and perturbations, we use a "one-way flux correction" as in Neelin (1990) to construct a known climatological state for the system. The ocean model is spun up to a steady state forced by a climatological wind stress and anomalies are defined with respect to this climatological steady state. The atmospheric model is used to obtain stress anomalies in response to SST anomalies for coupling.

Noting that only near-equatorial stress is important to this ocean model climatology, we use an idealized wind stress that approximates the observed annual average zonal stress near the equator:

$$\tau_c = 0.06\left\{0.1 - \cos^2\left[\left(\frac{x - x_0}{x_0 - x_W}\right)\frac{\pi}{2}\right] - 0.5\sin^2\left[\left(\frac{x - x_1}{3(x_E - x_W)}\right)\frac{\pi}{2}\right]\mathscr{H}(x - x_1)\right\}S_c(y) \quad (12)$$

in pascals, with $x_W = 130°\text{E}$, $x_E = 90°\text{W}$, $x_0 = 150°\text{W}$, $x_1 = 130°\text{W}$, and $\mathscr{H}(x - x_1)$ the Heaviside function. The last term of (12) departs from observed stress near the eastern boundary to give a more realistic climatology in this region, where processes not included in the model are active; $S_c(y)$ decays slowly with latitude with a Gaussian form. The resulted upwelling, w, thermocline depth, h, and SST of this solution are shown in Fig. 1. It gives a reasonably good simulation of the observed fields near the equator. Changing the oceanic parameters will alter this state slightly, but the general features do not change. Because it is in a steady state and the oceanic damping is very weak, the contribution of the shallow water layer motion to the advection and upwelling is small. The mean upwelling, thermocline depth, and SST are largely controlled by the surface-layer currents and the Sverdrup balance.

To couple the atmospheric component with the oceanic model, we take

$$\tau = \tau_c + \tau'(x)S(y), \quad (13)$$

where $\tau'(x)$ is the anomalous wind stress along the equator produced by the atmospheric model response to SST perturbations and $S(y)$ is a prescribed meridional structure. Because atmospheric meridional scales tend to be much larger than the oceanic Rossby radius, L_0, we expect meridional structure not to be of crucial importance. It has been shown by CMZ, however, that it can have some impact on the destabilization of coupled modes in some regimes. To test such effects, we use $S(y) = \exp(-\alpha y^2/2L_0^2)$, where α is related to the ratio of the oceanic Rossby radius to atmospheric meridional scales. The same form is used for $S_c(y)$. A value of $\alpha = 0.1$ is reasonable and is used throughout this study. Even for $\alpha = 0$, similar results are obtained in terms of the connections of eigensurfaces. The effect on destabilization of oscillatory modes noted by CMZ does hold here when thermocline feedbacks dominate.

The anomaly wind stress τ' is obtained by using (11) and defining SST anomalies as

$$T' = T - \bar{T}, \quad (14)$$

where $\bar{T}$ is SST of the model climatological state driven by τ_c. For sufficiently small μ, the climatological state is unique and the coupled system always decays to it.

The only aspect in which the ocean model as used for climatology and perturbation differs is that, for convenience, we introduce another free parameter δ_s that controls the anomalous surface-layer currents due to coupling. This parameter can be reduced from unity to zero without affecting the climatology. Because (4) is linear, this can be done by setting

$$w_s = \bar{w}_s + \delta_s w'_s$$
$$u_s = \bar{u}_s + \delta_s u'_s. \quad (15)$$

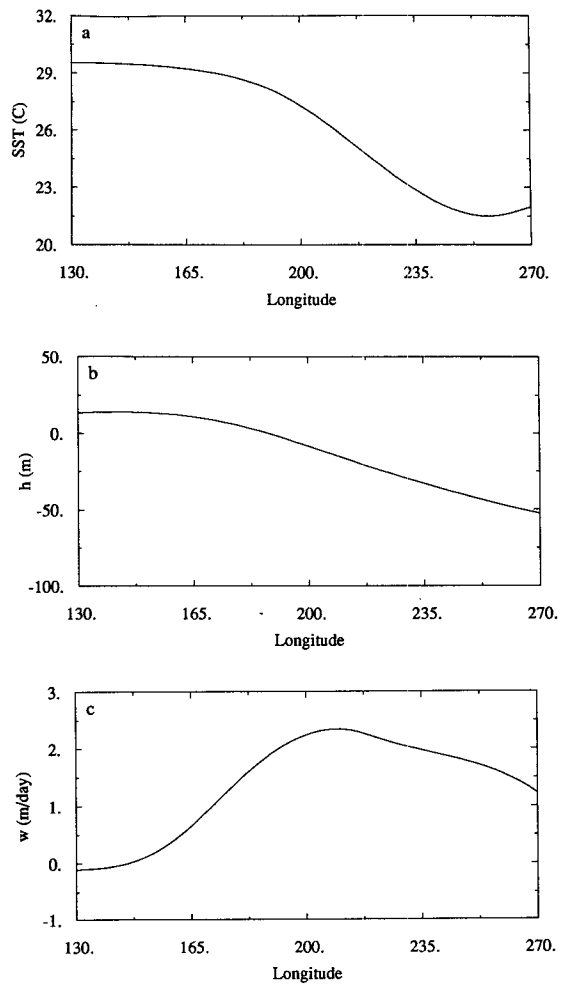

FIG. 1. Basic-state quantities at the equator: (a) SST, (b) thermocline departure from no-motion value (note negative values correspond to shallower thermocline), (c) upwelling.

d. *Linearization and parameter space*

In this coupled model, only the SST equation is nonlinear. To avoid the discontinuity arising from differentiating the Heaviside function, we use an analytic version

$$\mathscr{H}(w) = \frac{1}{2}(1 + \tanh(w/w^*)) \quad (16)$$

that approaches the true Heaviside function for small w^*. This simplifies linearization near regions with $w = 0$ and makes the nonlinear model everywhere infinitely differentiable. We use a simple numerical dif-

ferencing method to obtain the linearized system about the climatological state and examine eigenmodes with temporal dependence $e^{\sigma t}$. Spatial dependence is given by the eigenvector associated with each eigenvalue, σ.

For consistency, the oceanic parameters that determine the basic-state solution of Fig. 1 are not subject to further change once the basic state is obtained. The free parameters, which do not affect the basic state, are the relative coupling coefficient, μ, the atmospheric spatial damping scale, ϵ_a, and the two parameters, δ and δ_s, in the ocean model as introduced above. In the following sections we will discuss how the various coupled modes are related in this parameter space. We note that μ, δ, and δ_s are purposefully chosen to condense the most important effects of a number of physical processes into a few scalar parameters. To summarize: the range μ from 0 to 1 represents going from the uncoupled system to coupling which is at the strong side of the realistic range. Similarly, δ_s from 0 to 1 represents surface-layer feedbacks having no effect to having very strong effects, where we use the terminology *surface-layer feedbacks* to denote coupled feedback mechanisms involving the component of surface currents and upwelling produced by the embedded surface layer. The range δ from 0 to ∞ represents time scales for oceanic dynamical adjustment being much faster to much slower than the net time scale arising from the SST equation.

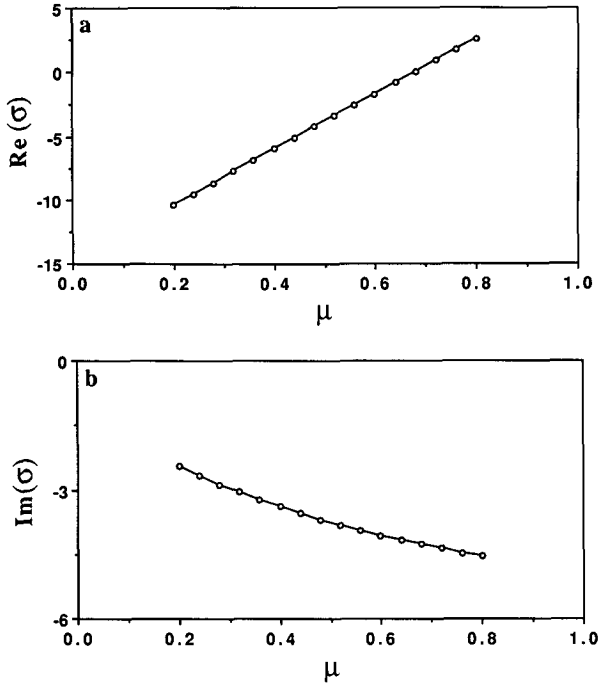

FIG. 2. Eigenvalue (in units of yr^{-1}) of the leading mode in the fast-wave limit ($\delta = 0$) vs relative coupling coefficient μ with $\epsilon_a = 2.0$, $\delta_s = 0.6$. (a) Growth rate, Re(σ), (b) frequency, Im(σ). For frequency, the convention of plotting only the negative root of the complex pair is used in all figures.

3. SST modes in the fast-wave limit

The physical interpretation of coupled modes is complicated by the presence of several processes participating in both the instability and oscillation mechanisms (Hirst 1988; BH; N91). Before considering the most realistic—and most complicated—part of parameter space, it is useful to consider a specialized limit in which the time scales of wave dynamics are, by definition, unimportant. This fast-wave limit case will prove particularly tractable in the analytical work of Parts II and III. Here we present the numerical fast-wave limit eigenmodes corresponding to the more realistic parameter range considered in the next section. A nonlinear version of a fast-wave limit model is outlined at greater length in HNJ.

a. *Relation of westward-propagating and stationary modes*

Figure 2 shows the growth rate and frequency of the leading eigenvalue as a function of relative coupling coefficient for a case where the surface-layer feedback is quite strong. This coupled SST mode becomes unstable when the coupling is strong enough, with both growth rate and frequency depending almost linearly on the coupling. An e-folding time of a few months and a period of 1 1/2 to 2 years occurs for moderate coupling around $\mu = 0.7$ and $\delta_s = 0.6$. The corresponding anomalous SST, upwelling, and thermocline fields along the equator for the unstable mode are shown in Fig. 3. These time–longitude plots are constructed from the linear solution using the eigenvector and frequency but with the growth rate suppressed, that is, $(X(x) \exp[i\,\mathrm{Im}(\sigma)t] + \text{c.c.})$, where $X(x)$ is the complex eigenvector, which contains spatial structure, and c.c. denotes the complex conjugate. We note that it is the combination of the eigenvector with the frequency, Im(σ), that determines propagation characteristics; eigenvectors and eigenvalues occur in conjugate pairs but both contain the same information. Near the bifurcation, such plots will correspond closely to the weakly nonlinear solution. SST and upwelling anomalies propagate westward in a coherent pattern, with relative upwelling/downwelling slightly to the west of cold/warm anomalies. The thermocline anomalies exhibit a slightly more complicated pattern, but in the central and eastern part of the basin thermocline anomalies propagate westward in association with SST; deep/shallow thermocline anomalies occur slightly to the east of warm/cold SST anomalies. The zonal phase shifts of upwelling and thermocline perturbations are due to a combination of atmospheric and (steady) ocean dynamics and behave much as in the zonally periodic case of N91. Both contribute to growth of the mode but compete in terms of the direction of propagation: the thermocline feedback tends to create eastward propagation, the upwelling feedback westward

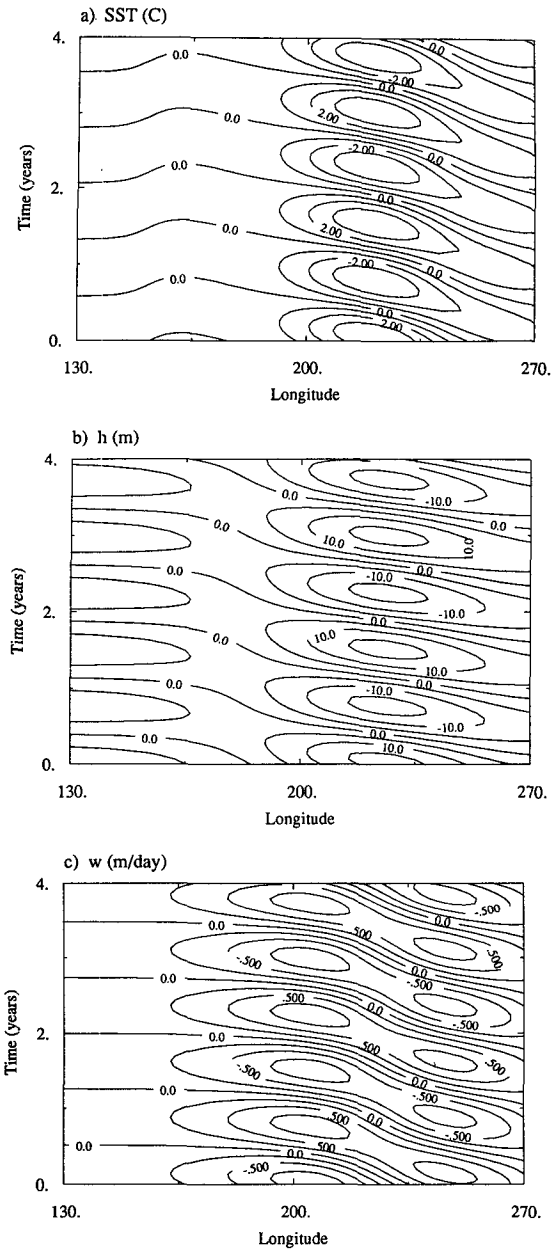

FIG. 3. Time–longitude plot of a westward-propagating SST mode in the fast-wave limit: (a) SST, (b) thermocline depth, (c) upwelling anomalies along the equator constructed from the eigenvector with growth tendency suppressed for $\mu = 0.7$ and other parameters as in Fig. 2 (units: °C, m, and m day^{-1}, respectively, up to a normalization factor).

propagation; and in this case the latter wins. An analytical treatment of these respective mechanisms in a finite basin may be found in Part III and a more detailed parameter dependence in the fast-wave limit for nonlinear cases is given in HNJ.

The features of this oscillation including the period and growth rate, eastern-basin trapping, and slightly westward propagation qualitatively resemble some aspects of the interannual variability simulated in GCMs and also to some extent the features of El Niño events (e.g., Rasmusson and Carpenter 1982). Although in reality ENSO events are much more complicated with occurrence of both westward propagation and stationary growth of SST anomalies (and arguably even eastward propagation in 1982–83), it is plausible to suggest that the above mechanism is one of the candidates operating in the ENSO phenomenon.

Given that processes with eastward and westward propagation tendencies compete in this mode and are modified by finite-basin effects, it is not surprising to find that as the surface-layer feedback is weakened, westward propagation slows and eventually the mode becomes stationary. Figure 4 shows this behavior. As δ_s is reduced to about 0.5, the frequency decreases to zero; the complex conjugate pair of oscillatory eigenvalues are reduced to an algebraically degenerate pair at this value of δ_s, that is, a 2-degeneracy with a single eigenvector (see Appendix). For lower values of δ_s, the two degrees of freedom previously associated with the conjugate pair appear as two stationary modes, with increased/decreased growth rates, respectively. Thus, the most unstable westward-propagating mode and the most unstable stationary mode in the two regimes on either side of $\delta_s \approx 0.5$ are part of a continuously connected surface of eigenvalues in parameter space. It can be convenient to think of them as, loosely speaking, the same mode in two regimes of behavior. Because

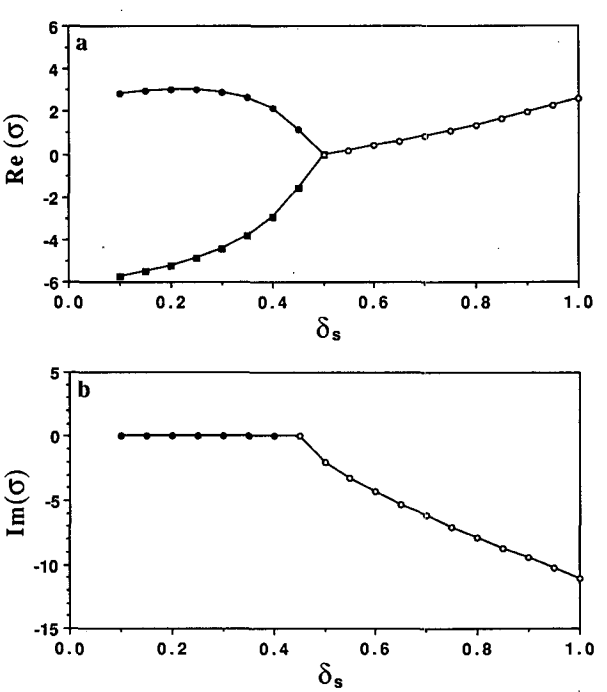

FIG. 4. Eigenvalue (yr^{-1}) of the leading SST mode(s) in the fast-wave limit vs surface-layer feedback parameter δ_s, for $\mu = 0.7$ and $\epsilon_a = 2.0$. (a) Growth rate, (b) frequency (negative root). Oscillatory values (open symbols) are westward propagating.

this 2-degeneracy is pure real, it extends as a continuous surface of dimension $(k-1)$ in a k-dimensional parameter space (see Appendix); this same surface, forming the boundary between stationary and westward-propagating modes, can therefore be encountered by varying parameters other than δ_s, or by replacing δ_s with related but more complex parameters. In qualitative terms, it is thus possible to take δ_s as a surrogate for any of these situations. Although not shown here, other westward-propagating modes can sometimes coexist with the stationary mode for the same parameter values (see HNJ).

b. *Stationary SST mode without surface-layer feedback*

The stationary, most unstable mode that occurs for $\delta_s < 0.5$ in Fig. 4 has properties that change relatively little as $\delta_s \to 0$, that is, as the feedback associated with anomalous surface-layer currents is turned off. It is thus useful to consider the simple case $\delta_s = 0$ to examine the behavior of the leading mode, beginning from this stationary case in the fast-wave limit. Stationary, that is, nonoscillatory, instabilities of the linear system are associated with multiple stationary states in the nonlinear system (e.g., see HNJ). In this case, a physically more important application can be guessed in advance based on physical intuition: if an unstable mode is stationary in the fast-wave limit, then it may become oscillatory as time scales due to ocean wave dynamics are introduced, away from the fast-wave limit. How this happens will be the subject of section 4.

Figure 5 shows the pure real eigenvalue of this stationary SST mode as a function of relative coupling coefficient. The stationary mode exists for the whole range of the coupling coefficient and becomes unstable for sufficiently strong coupling, with growth rate increasing quickly on the strong coupling side. Physically, the dominant instability process is the thermocline feedback in the SST equation. Typical SST and h fields of this eigenmode are shown in Fig. 6. The SST pattern is essentially of single sign (chosen positive here) with a broad maximum in the eastern part of the basin. It

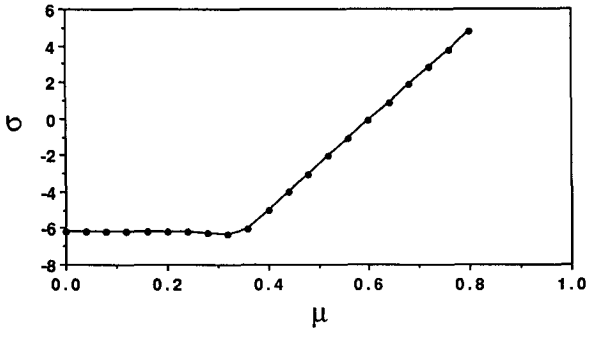

FIG. 5. Growth rate (yr^{-1}) of the leading stationary SST mode in the fast-wave limit vs relative coupling coefficient, μ, for $\delta_s = 0$ and $\epsilon_a = 2.0$.

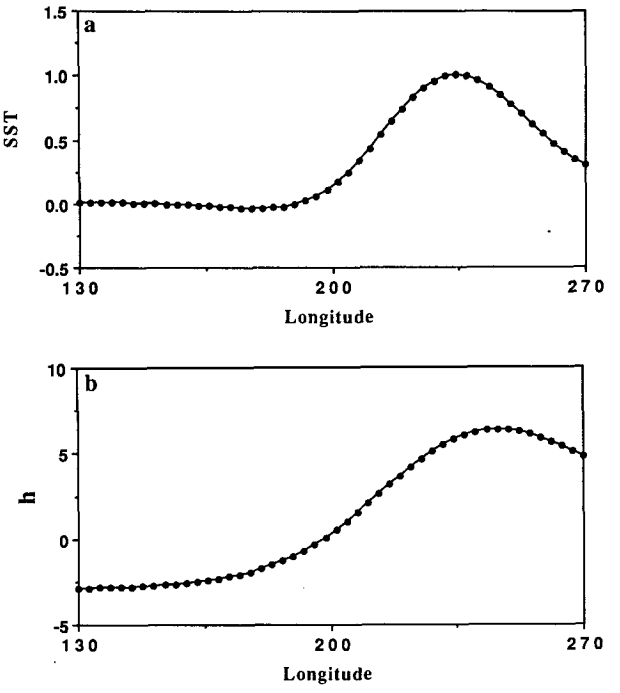

FIG. 6. Eigenfunction for the stationary SST mode for $\mu = 0.8$ and other parameters as in Fig. 5: (a) SST, (b) thermocline depth anomalies (units: °C and m, respectively, up to a normalization factor).

resembles the SST pattern of a warm (or, with sign reversed, cold) phase of the ENSO cycle, particularly as simulated in models such as CZ or Battisti (1988). The trapping of the SST response in the eastern half of the basin is influenced by the zonal dependence of the basic-state upwelling and subsurface temperature. Further east-basin trapping results from the east–west asymmetry due to the effect of β on ocean dynamics, expressed through the thermocline feedback, as examined at length in Part III (section 4).

c. *Relationship of stationary and eastward-propagating modes*

The existence of this stationary SST mode through a significant range of parameters (e.g., in Fig. 4) is the result of zonal symmetry breaking relative to the periodic-basin case considered in N91. In a zonally homogeneous ocean, stationary growth occurs only for particular parameter values that yield an exact balance of eastward and westward propagation tendencies. In the finite-basin case, zonal variations in the basic state and, especially, boundary conditions on ocean dynamics lead to purely growing modes occurring across a finite range of parameters. The thermocline feedback acting alone gives eastward propagation in the periodic-basin case. In the finite basin it can also do so, but only if the phase relation of wind stress and SST anomalies favors this tendency sufficiently strongly compared to

the effects of basin boundary conditions. We provide a numerical example here for comparison to analytical versions in Part III.

Figure 7 shows the eigenvalues of the two leading modes as a function of the inverse atmospheric damping length, ϵ_a, which affects the phase relation between SST and wind, as well as the spatial correlation scale due to atmospheric effects. As ϵ_a becomes larger (i.e., the atmospheric spatial damping scale becomes smaller), the most unstable stationary mode merges with the least rapidly decaying stationary mode at another 2-degeneracy to yield an unstable eastward-propagating mode, whose period decreases rapidly from infinity to about 2 to 3 years. A typical eigenfunction for this mode is shown in Fig. 8. Both the SST and thermocline patterns are very similar to those of the stationary mode and it has a striking stationary oscillation component; the SST and thermocline anomalies are trapped to the east coast for related reasons. Upwelling anomalies are unimportant, as in the stationary case. Thus, this eastward mode can usefully be thought of as a modification of the stationary SST mode, perturbed by propagation tendencies that are qualitatively the same as the periodic-basin case. That is, the thermocline feedback can yield eastward propagation through phase lags between T' and τ', and between τ' and h', such that thermocline shallowing and deepening are slightly to the east of warm and cool SST anomalies, respectively.

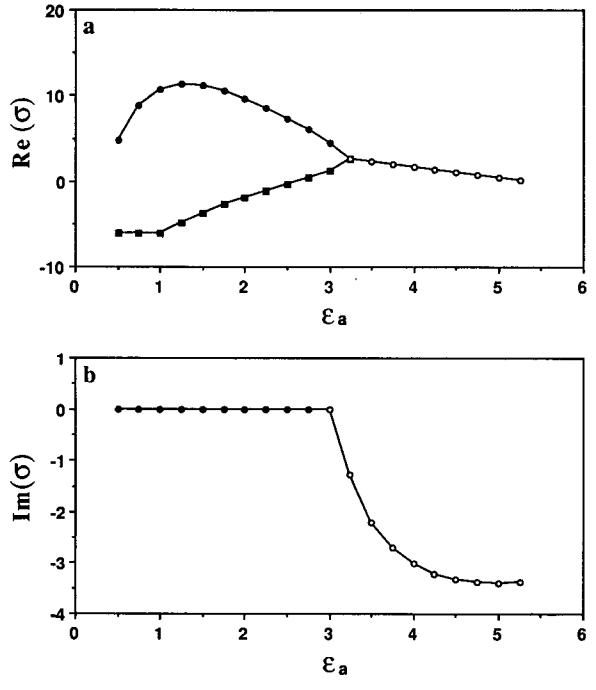

FIG. 7. Eigenvalue (yr^{-1}) of the leading SST mode(s) in the fast-wave limit vs atmospheric damping coefficient ϵ_a for $\delta_s = 0$ and $\mu = 1.0$. (a) Growth rate, (b) frequency (negative root). Oscillatory values (open symbols) are eastward propagating.

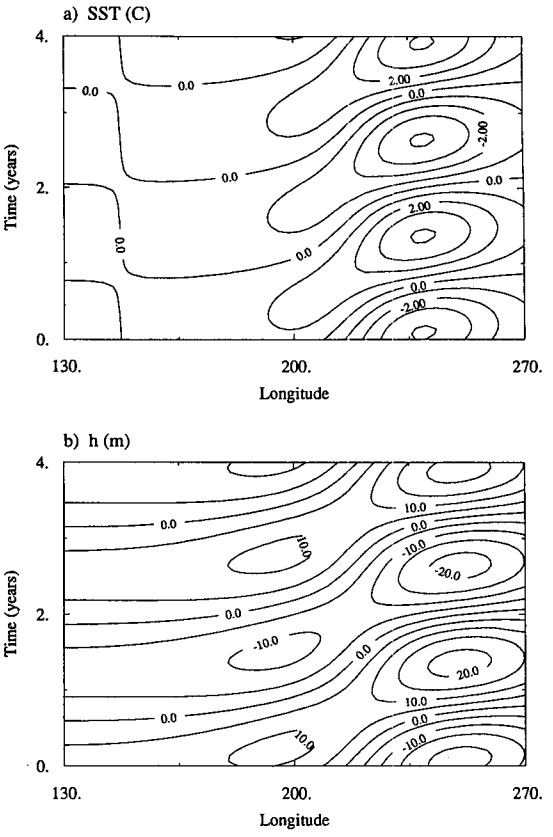

FIG. 8. Time–longitude plot of an eastward-propagating SST mode in the fast-wave limit: (a) SST, (b) thermocline depth anomalies along the equator constructed from the eigenvector for $\mu = 0.9$, $\delta_s = 0$, and $\epsilon_a = 4.0$ (units: °C and m, respectively, up to a normalization factor).

The relation of the most unstable westward- and eastward-propagating modes to the stationary mode in their respective parameter regimes provides further motivation for beginning our explorations from this stationary mode when considering cases away from the fast-wave limit. Because the propagating modes possess oscillation mechanisms that do not depend on wave time scales in the fast-wave limit, the stationary mode will prove a much simpler case for unraveling how oscillation can arise from effects of oceanic adjustment.

4. Mixed SST/oceanic dynamics modes

The role of ocean wave dynamics in modes of coupled variability has long been discussed, usually in terms of the uncoupled Rossby and Kelvin modes of a longitudinally periodic ocean. Instability analysis in periodic basins shows that coupled versions of these waves may indeed be destabilized (Philander et al. 1984; Yamagata 1985; Hirst 1986; N91). In a finite basin, however, coupled modes closely related to individual Rossby and Kelvin waves occur mainly in situations of high frequency (e.g., Kelvin wave secondary instability of Neelin 1990) or large effective damping (Hirst 1988). In a zonally bounded ocean basin,

boundary reflections imply that even the uncoupled modes of the system will consist of sums of Kelvin and Rossby waves, which can be quite different from the x-periodic case, especially at low frequency and basin scale. The modes of the uncoupled shallow-water equations (in the long-wave approximation) consist of two classes: the ocean basin modes of Cane and Moore (1981) (which would be "leaky" solutions in the full shallow-water equations) and an overlooked class of decaying "scattering modes," which we derive in appendix A of Part II. By scattering modes we simply mean free modes for which energy must be incident into the system, for example, equatorward along the western boundary, since leakage occurs poleward along the eastern boundary. Under the long-wave approximation in conventional series representation, the continuum spectrum is discretized. For truncation N in the meridional and with K degrees of freedom in the zonal direction, there are K ocean basin modes and $(N - 1)K$ scattering modes. The scattering spectrum is needed for completeness (in terms of representing initial conditions). Because of energy leakage, these modes damp faster than the local physical decay rate in the uncoupled problem. However, because some of the scattering modes have low frequencies, they can enter into the coupled problem. In the uncoupled case for our model, there will also be a decaying set of SST modes.

In this section, we examine the relation of modes in the most realistic part of parameter space to those in the relatively simple cases of the fast-wave limit and the uncoupled ocean. One may anticipate that the modes will have a mixed character, and it is of interest to know just how they are constructed.

a. Relation of stationary SST mode and standing oscillation due to wave dynamics

For simplicity, we focus on the case without mixed-layer feedback, that is, setting $\delta_s = 0$. We examine the behavior of the few leading (fastest growing or slowest decaying) eigenmodes as a function of μ and δ. Figure 9 provides an orientation to the slices that will be presented in the μ–δ plane; we begin with the relatively simple situations that occur near the fast-wave limit (slice 1) and at moderately strong coupling (slice 2), then proceed to the case closer to the fast-SST limit (slice 3) before showing the more complex cases in between (slices 4 and 5).

Figure 10 shows slice 1 ($\delta = 0.5$) in two formats. Figures 10a and 10b give the growth rate and frequency as a function of μ for the two leading modes; the other modes are decaying relatively quickly. As in the fast-wave limit, only a single mode (solid dots) becomes unstable at strong coupling, which is a stationary, purely growing mode. The second mode is oscillatory (open circles), with frequency shown in Fig. 10b. It is destabilized by coupling relative to the zero-coupling

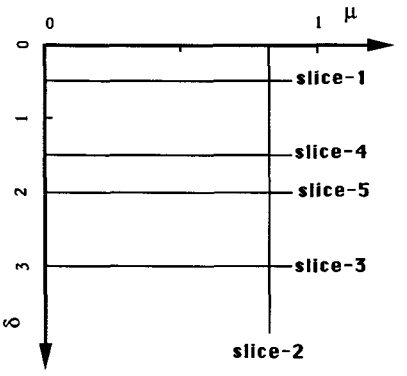

FIG. 9. Schematic of the μ–δ plane (coupling coefficient and relative time-scale coefficient) showing the slices for which eigenvalues will be presented in Figs. 10, 11, 13, 15, and 16. Slices are labeled in order of presentation.

end, but never becomes unstable. It remains distinct from the leading stationary mode throughout the range of coupling shown. At zero coupling, it turns out to be the lowest-frequency mode of the discretized scattering spectrum.

Figure 10c provides a more complete view along this same slice, condensed by plotting the eigenvalues of the five leading modes on the complex plane, for the coupling values in the range $\mu = 0$ to 0.8. The eigenvalues trace out a continuous path as a function of μ. For this value of δ, these paths remain distinct for all modes. The left–right symmetry about $\mathrm{Im}(\sigma) = 0$ is because oscillatory modes always exist as complex conjugate pairs. There are four pairs of curves of the oscillatory modes, with very different frequencies at all values of coupling. The origin of these modes is thus conveniently stated in terms of their identities at $\mu = 0$, namely, the scattering modes, and a smaller number of ocean basin modes. The pair of modes with the highest frequency shown are the gravest ocean basin modes, and the other three pairs are the gravest scattering modes with considerably lower frequency. Although all oscillatory modes in this case are stable, the pair of scattering modes with lowest frequency is most nearly destabilized and tends to approach the stationary mode for intermediate coupling values ($\mu \sim 0.6$, see also Fig. 10a,b) an indication of the increasing mixing of properties between ocean modes and SST modes away from the fast-wave limit as δ increases.

The similarity of the unstable stationary mode to the SST mode of Fig. 5 suggests that the transition from the fast-wave limit to this case is smooth. This is true except for one subtlety. At very low μ and δ, there is a merger that is best described as the SST mode absorbing a degree of freedom associated with mean thermocline displacements. Specifically, the $h = \text{const}$ solution of the uncoupled ocean is not a solution for finite coupling due to its effects through the SST equation. Its structure, and that of the uncoupled SST modes, is rapidly modified by even very small coupling

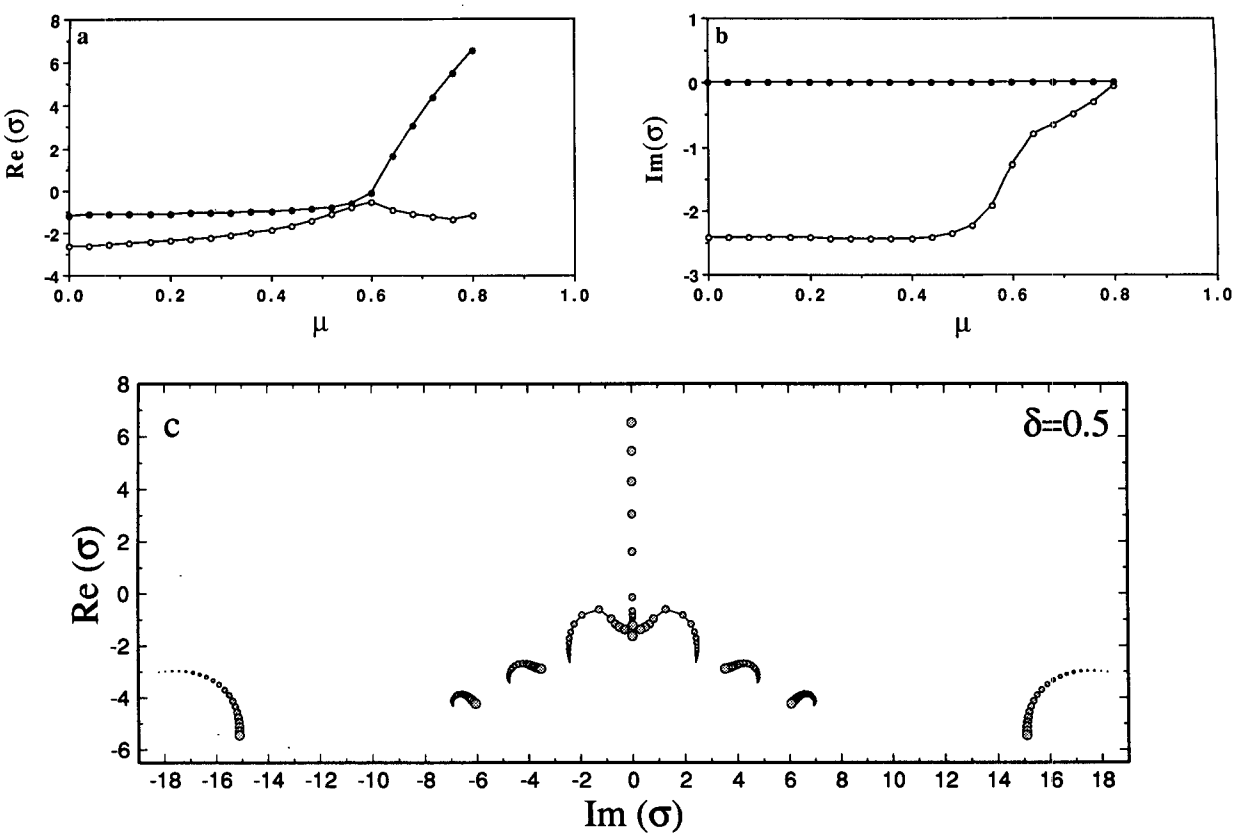

FIG. 10. Eigenvalues of the leading modes vs relative coupling coefficient, μ, for $\delta = 0.5$, $\delta_s = 0$, and $\epsilon_a = 2.0$ (slice 1 of Fig. 9). (a) Growth rates of the two leading modes, (b) frequencies (negative or zero roots) of the two leading modes. In (a) and (b) solid or open symbols are used for pure-real or oscillatory eigenvalues, respectively. (c) Collective plot of the five leading modes on the complex plane for coupling values at equal intervals in the range $\mu = 0$ (smallest dots) to 0.8 (progressively larger dots denote correspondingly larger μ). Paths of continuous connection are indicated by interpolated lines wherever clarification is needed for the μ-spacing shown. Eigenvalues are in yr^{-1} as redimensionalized by the SST time scale; to get values redimensionalized by the ocean-dynamics time scale, multiply by δ.

(see Part II, section 4). At moderate and high coupling the mode shown in Fig. 5 is virtually identical to the dominant SST mode in the fast-wave limit, but at low coupling this merger results in a reduced decay rate. It may be recalled from Fig. 6 that this SST mode does indeed have a strong mean thermocline depth component.

Before presenting a number of more important mergers that occur at low and intermediate coupling, it is helpful to note that these complications disappear as coupling becomes slightly stronger, roughly for $\mu > 0.6$. For strong coupling, the strongly growing stationary mode of Figs. 5 and 10 stands out from all other modes and can easily be traced as a function of δ. Figure 11 shows the (pure real) eigenvalue of this mode along slice 2 of Fig. 9. The crucial feature of this figure is that the eigenvalue encounters no degeneracies and no qualitative changes between $\delta = 0$ and large δ. Thus, the eigenvalue surface of the leading unstable mode toward the strong coupling side smoothly spans the whole range of the parameter domain for the relative time scale ratio, from the fast-wave limit to the fast-SST limit. Figure 12 shows the SST component of the corresponding eigenvector for two well-separated values of δ, one near the fast-wave limit and one toward the fast-SST limit; the structure changes little throughout the range. The reason for the robustness of this mode at stronger coupling is that the feedback processes

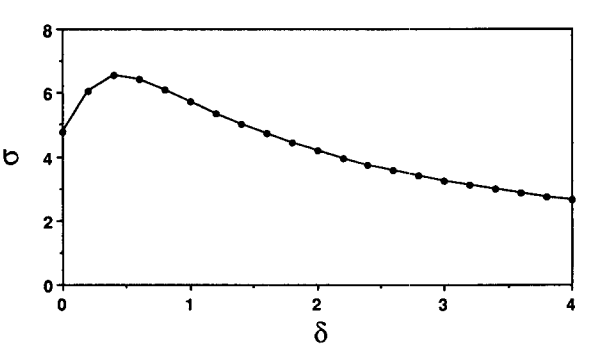

FIG. 11. Growth rate (yr^{-1} by SST time scale) of the (pure real) leading mode vs relative time-scale coefficient, δ, for $\mu = 0.8$, $\delta_s = 0$, and $\epsilon_a = 2.0$ (slice 2 of Fig. 9).

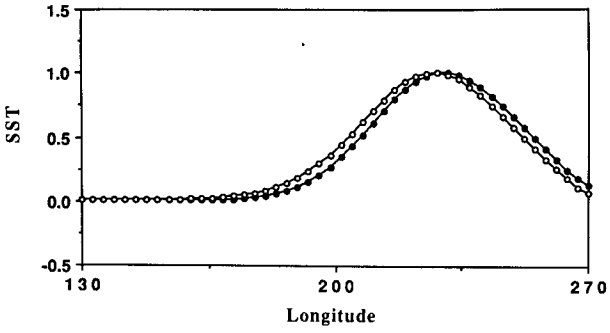

FIG. 12. SST component of the eigenfunction for the stationary SST mode at $\delta = 1.0$ and $\delta = 3.0$, for other parameters as in Fig. 11.

are so strong that local growth dominates over wave propagation processes, as elaborated in Part III. As discussed in section 3, the physics of the SST mode at the fast-wave limit is relatively simple and easily understood. The continuity shown here demonstrates that the fast-wave limit is an ideal special case to understand the underlying dynamics of this strongly growing stationary mode.

Away from the fast-wave limit, the strongly growing stationary mode contains ocean dynamical time scales; one may anticipate that this must connect somehow to the uncoupled case where these occur in oscillatory oceanic dynamics modes. The parameter regime near the fast-SST limit is more complicated than near the fast-wave limit but still simpler than for intermediate δ. An example with $\delta = 3.0$ (slice 3) is shown in Fig. 13. Comparing Fig. 13a with Fig. 10a, an obvious similarity is found for the strongly growing mode at strong coupling, $\mu > 0.6$, due to the continuous connection from the fast-wave limit discussed above. However, the connection between this branch and low coupling is now complicated by the presence of a number of degeneracies at which different eigensurfaces join. In this case, each 2-degeneracy joins a complex branch with two degrees of freedom (open symbols) to two pure-real branches (solid symbols) in a locally quadratic dependence (see Appendix). The pure real branch at low coupling (solid squares in Fig. 13a,b) no longer connects continuously to the pure real branch at strong coupling as it did in Fig. 10a. Rather, an oscillatory branch (open circles), that begins as an ocean basin mode at $\mu = 0$, is strongly modified by the coupling; as coupling increases, the growth tendency increases, frequency decreases, and the eigenstructure changes to more resemble that of the strongly growing branch, eventually becoming identical as the frequency drops to zero at the 2-degeneracy. Slightly to the strong coupling side of the 2-degeneracy, there is a region where all three eigensolutions are real, until the lower growth-rate branch emerging from the first 2-degeneracy merges in a second 2-degeneracy with the decaying stationary mode to form a decaying oscillatory mode (the feature at higher coupling where this again breaks into two decaying real modes is of little significance).

To see how the other modes behave, a plot of the top five eigenmodes is shown in Fig. 13c, similar to Fig. 10b except with coupling from 0 to 1. The three branches of oscillatory, decaying modes related to scattering modes, which correspond to the three discussed in Fig. 10b, are well separated from the more unstable branches. The branch that begins at the uncoupled, decaying ocean basin mode (smallest dot at largest frequency) is attached to the stationary mode (on the real axis for all values of coupling—note that there is some overlap of dots for decaying real modes at high and low coupling), forming a set of connected surfaces. This contrasts to the situation near the fast-wave limit (Fig. 10c) where all modes remain distinct for all values of coupling. Figure 13 characterizes the fast-SST limit, since these features continue out to large δ without qualitative change. The fact that it is the two furthest separated modes in Fig. 13c that are connected hints at other mergers that must occur between these limits, as discussed below.

The merger of the strongly growing stationary mode with oscillatory modes from the ocean spectrum is of considerable consequence. Because the strongly growing stationary mode is smoothly connected with an SST mode at the fast-wave limit (as seen in Fig. 11), this merger represents the mixing of the two very different kinds of mode through coupling. In a broad neighborhood of the parameter space around such mergers, the behavior of the leading mode is of entirely mixed character, with features taken from the two ingredients, namely, an SST mode (the gravest in all cases shown here) and ocean-dynamics modes. We refer to these generically as "mixed SST/ocean-dynamics modes." Of course, all modes in the center part of parameter space, away from the specialized limits, have a mixed character to greater or lesser extent. For instance, while the stationary unstable mode on the strong coupling side of the degeneracy closely resembles the SST mode at the fast-wave limit, the dependence of growth rate on coupling has a more quadratic dependence in Fig. 13a rather than the near-linear dependence of Fig. 10 and Fig. 5. It will be shown in Part III that this is because the time scales of oceanic dynamics participate in the dominant physical balances of this mode as δ becomes large.

On the weak coupling side of the degeneracy for the leading mode in Fig. 13, the eigenstructure evolves significantly as a function of coupling but retains features consistent with a combination of the uncoupled and strongly coupled behavior. Figure 14 shows an example of the eigenstructure typical of the "mixed" range where the oscillation is relatively slow and the mode tends to be destabilized. The exact point in parameter space is labeled A in Fig. 13. Time is given dimensionally according to the SST equation time scale for standard parameters but could be rescaled according to one's

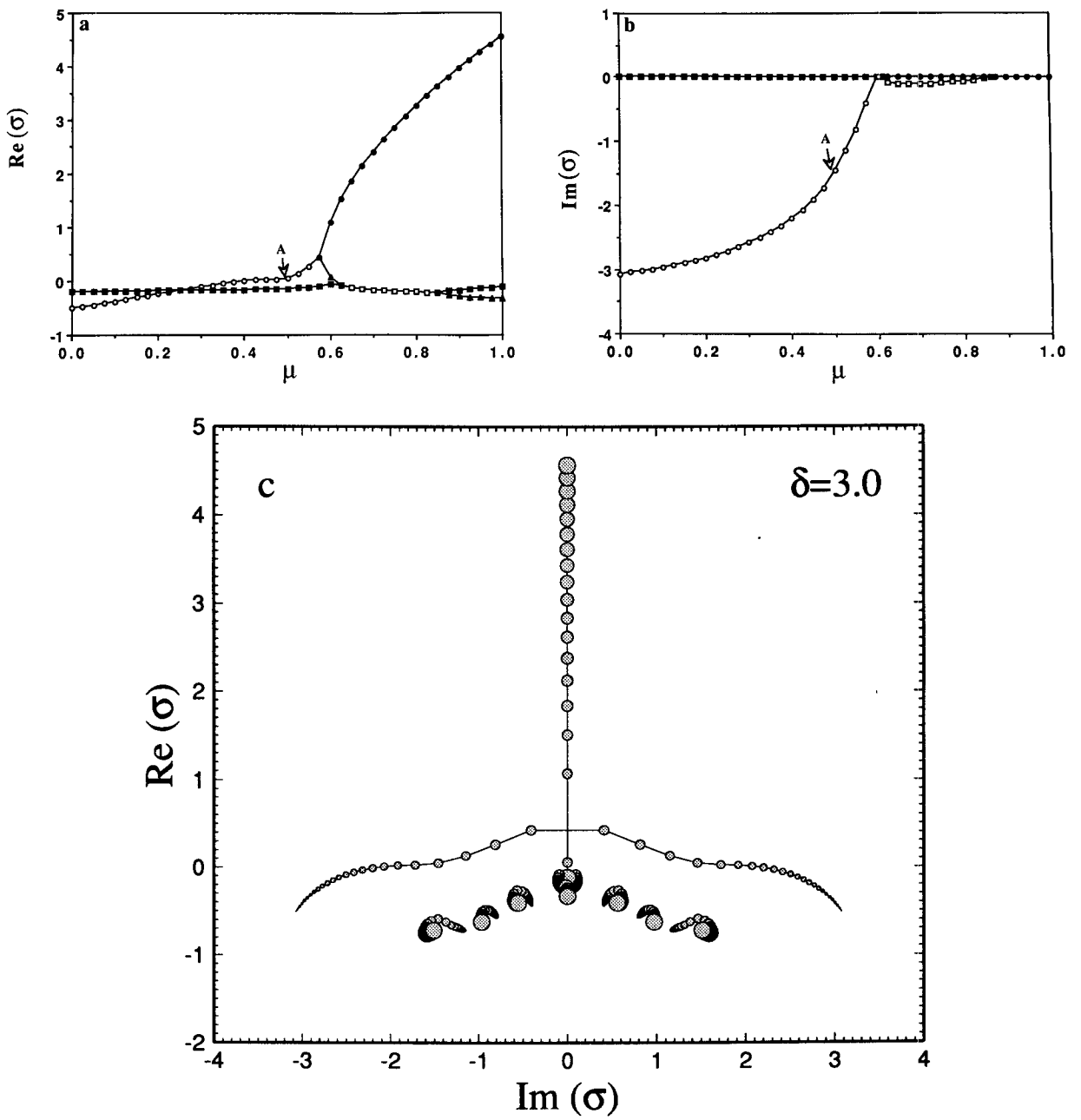

FIG. 13. As in Fig. 10 except for $\delta = 3.0$ (slice 3 of Fig. 9). (a) Growth rates of the two leading modes, (b) frequencies (negative or zero roots) of the two leading modes, (c) collective plot of the five leading modes. The label A marks the point for which the eigenstructure is shown in Fig. 14.

interpretation of $\delta = 3$ as faster SST time scales or slower wave time scales. The SST evolves in a standing oscillation, with a spatial structure that closely resembles the stationary mode of Fig. 12. The east-basin trapping can thus be understood from the fast-wave limit as discussed in section 3b and in Part III (section 4).

The thermocline depth in Fig. 14b has the characteristic pattern found, for instance, in the CZ coupled model or in the Chao and Philander (1993) diagnosis of an OGCM driven by observed winds: deep thermocline in the western Pacific leads deep thermocline and warm SST in the eastern Pacific by between one-half and one-quarter oscillation period. A slow eastward "propagation" in midbasin is associated with this transition, but at phase speeds far too slow to be associated with pure Kelvin wave propagation. This type of feature occurs quite generally for finite-basin ocean dynamics driven by large-scale wind patterns at frequencies lower

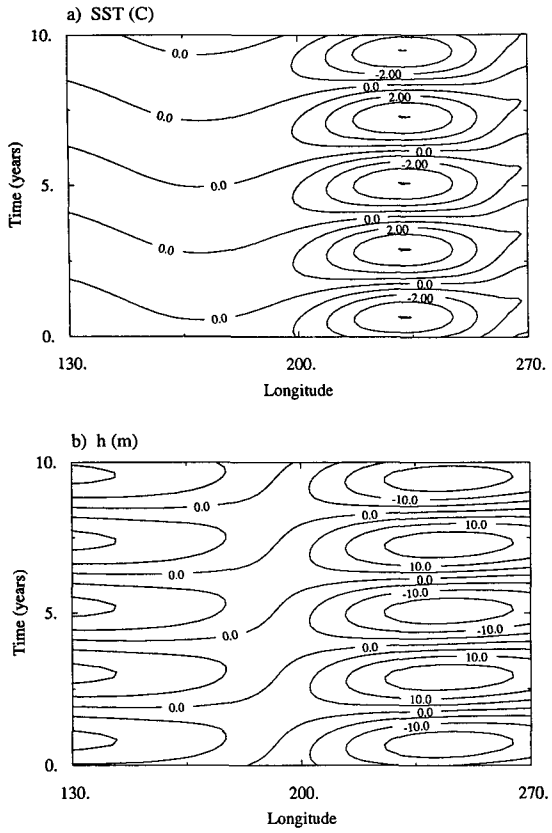

FIG. 14. Time–longitude plot of a mixed SST/ocean-dynamics mode for (a) SST, (b) thermocline depth anomalies along the equator, constructed from the eigenvector for the point labeled A in Fig. 13 (μ = 0.5, δ = 3.0). Units are °C and m, respectively, up to a normalization factor. Time dimensionalized by SST time scale.

than that of the gravest ocean basin mode (Cane and Sarachik 1981). In this case, the oceanic wave adjustment process associated with this feature is providing the memory for the coupled oscillation. As the degeneracy is approached and the period becomes very long, the form of the mode changes little except that the lag between east and west approaches half a period. As one tracks this mixed mode to low coupling, more substantial changes occur: the lag approaches one-quarter period, and the phase of the thermocline perturbation changes abruptly at exactly midbasin as is characteristic of the Cane and Moore (1981) ocean basin modes. Interestingly, the coupled case is much better behaved and more robust than the near-singular structure of the uncoupled case. The oscillation for the parameter values shown here (without surface-layer feedbacks) is dominated by the thermocline feedback. Upwelling is very small and zonal advection by mean currents contributes only modestly.

The overall behavior of the eigenmodes as a function of coupling shown in Fig. 13 and the eigenstructure of the leading mode shown in Fig. 14 remain essentially the same for $\delta > 2$. Thus, near the fast-SST limit, the presence of a mixed mode connecting the gravest ocean basin mode with a strongly growing stationary mode is a coherent feature, at least for some range of small δ_s. This is consistent with the results of the CMZ fast-SST-limit model (coupled through the thermocline feedback at a single point). Our results show that there is indeed a significant range of parameters for which their model provides an excellent analog to the leading mode of the fuller system (as long as propagation tendency does not need to be taken into account). It is even possible to extend their system to permit a simple analog to the stationary SST mode, with similar connections to the fast-wave limit. It would therefore be convenient if the story could end here. Unfortunately, an additional complication arises in the most realistic part of parameter space, for slightly smaller δ.

For $\delta \leqslant 2$, the branch connected to the ocean basin mode does not become unstable and does not join the strongly growing stationary mode at stronger coupling. Instead, the strongly growing stationary mode is joined to oceanic dynamics modes from the scattering spectrum. In Fig. 15, we show a case with δ = 1.5 (slice 4 of Fig. 9). The branch connected to the ocean basin mode at zero coupling (open circles in Fig. 15a,b) is destabilized a bit as coupling increases but it decays before becoming unstable and does not connect to the other branches. The other two oscillatory modes (open diamonds and open squares) are identified at low coupling as the two lowest-frequency scattering modes. The one with smaller frequency (open diamonds) has a sudden increase in growth rate and decrease in frequency above $\mu \approx 0.5$. It is then connected at another 2-degeneracy to the strongly growing stationary mode (solid circles) plus a decaying stationary branch (solid triangles), which in turn joins the decaying stationary mode from low coupling (solid squares). Thus except for the fact that it is a scattering mode that joins the strongly growing stationary mode, the picture is very similar to that of Fig. 13a,b. The second branch that begins as a scattering mode at low coupling (open squares) does not merge with the other branches for this value of δ, but there is a region (around μ = 0.54) where both its growth rate and frequency closely approach that of the first scattering mode branch. This is a signature of further mergers at neighboring parameter values.

The joining of the first scattering mode with the strongly growing stationary mode is more vividly illustrated in Fig. 15c. The 2-degeneracy that connects the growing stationary mode to the oscillatory part of the spectrum in the center of the diagram is comparable to Fig. 13c, but the mixed oscillatory branch that arises from this connects to the nearest (i.e., lowest frequency) scattering mode at low coupling, in contrast to Fig. 13c where it connects all the way across to the ocean basin mode. It is easy to see how this diagram is closely related to that of Fig. 10b, near the fast-wave limit, where the modes all remain distinct, but where the branch as-

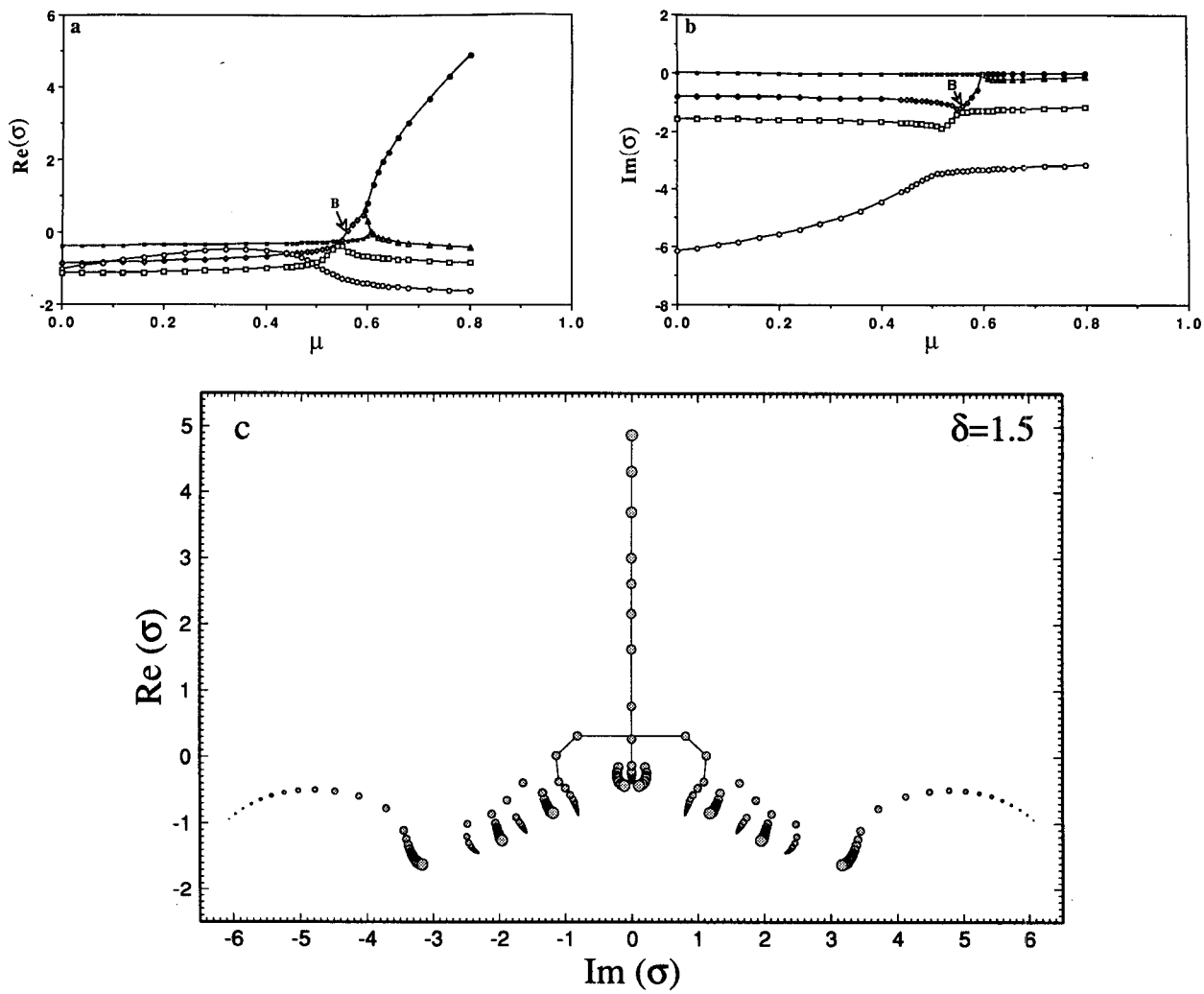

FIG. 15. As in Fig. 10 except $\delta = 1.5$ (slice 4 of Fig. 9) and (a) growth rates of the four leading modes, (b) frequencies (negative or zero roots) of the four leading modes; symbols denoting the same branch between (a) and (b) change at the 2-degeneracies for clarity (to distinguish from branches that cross without degeneracy) but mode properties are continuous. (c) Collective plot of the five leading modes. The label B marks the point for which the eigenstructure is shown in Fig. 17.

sociated with the lowest-frequency scattering mode closely approaches the stationary SST mode.

To better understand this connection, consider what happens as δ is reduced from 1.5. The qualitative behavior of Fig. 15 holds down to $\delta \approx 1$, except that the small range of coupling around $\mu = 0.6$ that has three real roots is reduced in size. The two 2-degeneracies at either end of the small branch denoted by solid triangles approach each other and merge into a 3-degeneracy, where all modes associated with these three degrees of freedom have the same structure. Below this δ value, the behavior is qualitatively like that of Fig. 10. This 3-degeneracy thus serves as a central point in the connection of the eigensurfaces. In Part III, we will argue that its existence is implied by the physical linkage of the SST modes to the strongly growing mode at strong coupling.

Now consider the connection between Fig. 15 and Fig. 13. In Fig. 15a, we pointed out a near merger of the branches associated with the first and second scattering modes. As δ is increased from 1.5, a degeneracy does occur that connects these two eigensurfaces. This is another 2-degeneracy, but because it has nonzero frequency it occurs only for a specific value of (μ, δ) as explained in the Appendix. For slightly larger δ, the mixed mode branch attached to the strongly growing stationary mode connects to the second scattering mode. As δ is increased further, another such degeneracy occurs, connecting this branch instead to the third scattering mode. Figure 16 shows this latter case for $\delta = 2$ (slice 5 of Fig. 9). The joining of the third scattering-mode branch with the stationary mode is clearly seen in Fig. 16c. The first two scattering-mode branches are decaying and detached. The branch arising from

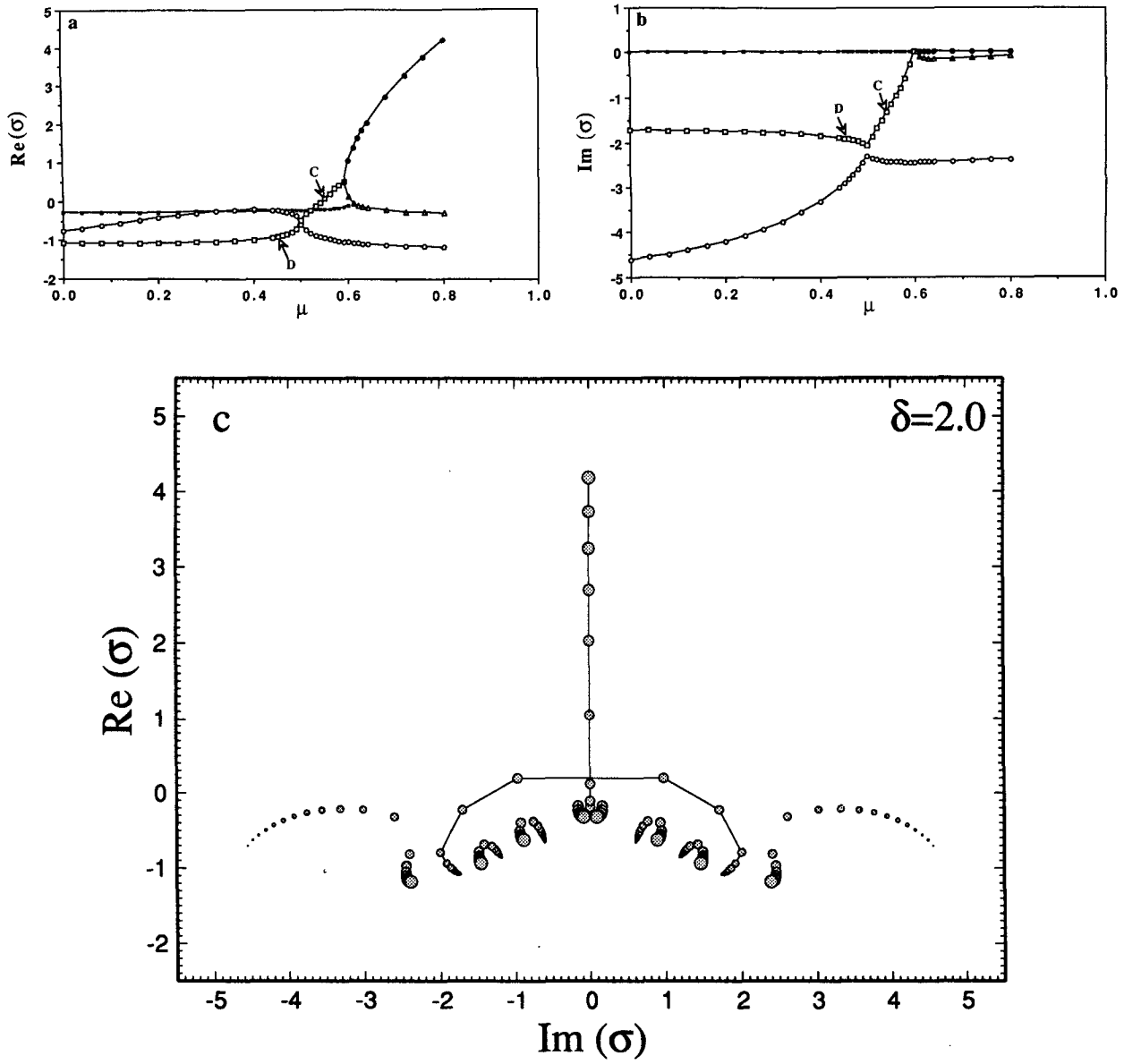

FIG. 16. As in Fig. 10 except $\delta = 2.0$ (slice 5 of Fig. 9) and (a) growth rates of the three leading modes, (b) frequencies (negative or zero roots) of the three leading modes, (c) collective plot of the five leading modes. The labels C and D mark the points for which the eigenstructure is shown in Figs. 18 and 19.

the ocean basin mode is still stable, but is close to the point of merging with the branch connecting the stationary mode to the third scattering mode. This merger occurs for δ slightly larger than 2 in a final 2-degeneracy, which leads to the behavior of Fig. 13.

A more detailed view of how this type of merger occurs may be obtained from Fig. 16a,b, in which the eigenvalues of the three leading modes are plotted. The strongly growing stationary mode branch (solid circles) and the 2-degeneracy that connects it to an oscillatory mixed mode (open squares) are essentially the same as in Figs. 13a,b and 15a,b. As one traces this oscillatory mixed-mode branch back toward low coupling (where it connects to the third scattering mode), it comes very close to merging at about $\mu = 0.5$ with the branch arising from the ocean basin mode (open circles). Note that the growth rate curves cross, but that the frequencies are not identical, although they approach each other at this point. There is a slightly larger value of δ at which a 2-degeneracy occurs where the frequency curves cross at the same time as the growth rate curves. The modes associated with the two branches are identical at this point. For δ values larger than that of the degeneracy, the frequencies cross but the growth rate

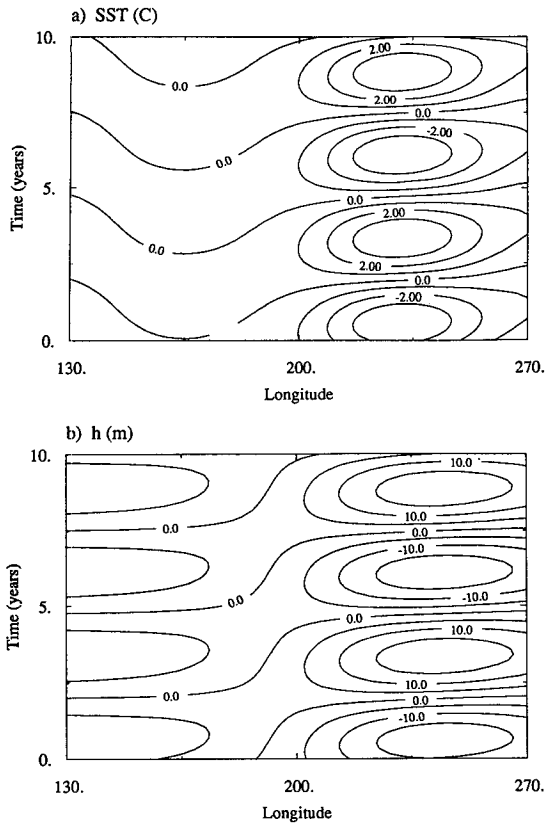

FIG. 17. As in Fig. 14 except for the point labeled B in Fig. 15 ($\mu = 0.55$, $\delta = 1.5$).

curves do not, although they dip toward one another. The behavior in the region of such a degeneracy is outlined in the Appendix.

This succession of three transitions between δ values of about 1 and just over 2 may create some concern in the reader who wishes to conceptualize the coupled modes in terms of the modes of the uncoupled ocean. This worry is multiplied if one recalls that the number of scattering modes in a numerical model is resolution dependent. Adding resolution in such a way as to increase the number of low-frequency, large spatial-scale scattering modes will simply increase the number of transitions required to get from the behavior of Fig. 15c to that of Fig. 13c. Thus, there appears to be nothing fundamental about which oceanic degree of freedom goes into the mixed SST/ocean-dynamics mode when it is destabilized.

Although this has important implications for how we view the system, it is inconsequential to the behavior of the mixed modes themselves. The eigenstructure of the oscillatory mode is robust through a substantial parameter range, from μ around 0.5, where the growth rate picks up sharply, to the merger with the stationary mode, and for δ from less than 1 to very large values, no matter which ocean branch is connected to it. Figures 17 and 18 show two eigenstructures for the cases of Figs. 15 and 16 (for the points labeled B and C on these figures, respectively). Although different oceanic modes are connected to the mixed branch at these two points, they have virtually the same structure. The period is sensitive to the coupling due to the fact that this mode is close to the merger with the stationary branch, but SST and thermocline perturbation patterns are coherent and very similar to that shown in Fig. 14. Furthermore, there is a dramatic change in the eigenstructures between low μ values where they are identified as scattering modes and the range of μ where the increase in growth rate signals the transition to mixed-mode behavior. The change in structure and growth rate is even greater than in the case of the connection to the ocean basin mode of Fig. 13. Figure 19 shows an example for a mode at lower coupling along the branch connected to the case of Fig. 18, at the point labeled D in Fig. 16. This decaying mode has very different h and SST (not shown) patterns. It is worth pointing out that this fundamental change in the physics of the mode is not directly associated with crossing any degeneracy surface; it may be contrasted to the relatively minor change in any properties except frequency at the transition to the stationary mode. Thus, the degeneracies should not be relied on completely to define boundaries between physical flow regimes.

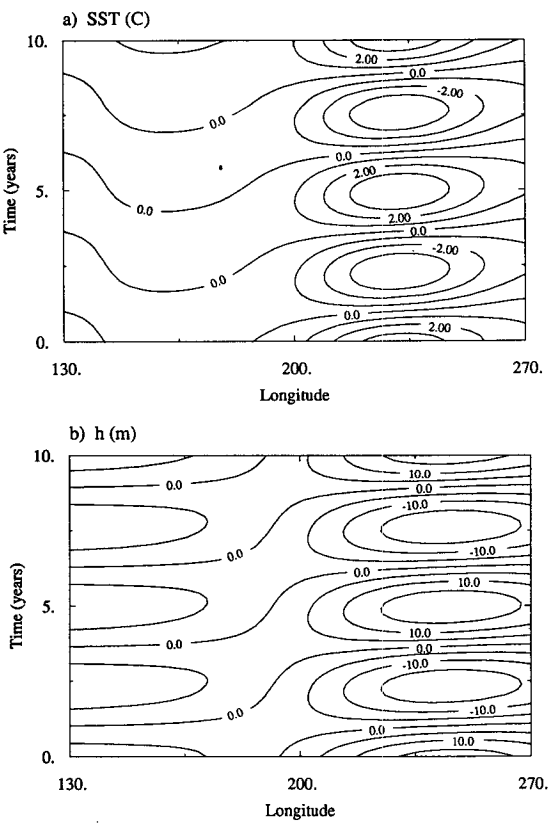

FIG. 18. As in Fig. 14 except for the point labeled C in Fig. 16 ($\mu = 0.55$, $\delta = 2.0$).

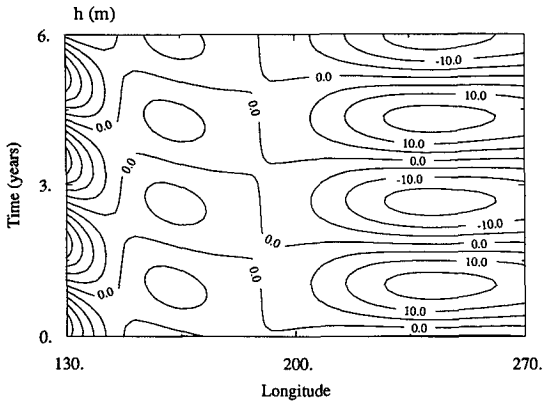

FIG. 19. As in Fig. 18 except for the point labeled D in Fig. 16 ($\mu = 0.45$, $\delta = 2.0$) and only h field shown.

The conclusion we are led to is that the coupled modes in the most important parameter range are best understood when approached from the strong coupling side. The eigenvalue and eigenstructure are coherent in a substantial neighborhood around the joining of the oscillatory mixed-mode branch to the vigorous stationary mode. Although this neighborhood may be limited to a relatively narrow range of coupling coefficient, as in Fig. 15 and Fig. 16, it is the range in which these modes can first go unstable. Furthermore, the structure of these modes is very closely related to that of the strongly growing stationary mode, aside from the small phase lags in the ocean dynamics that produce the period. The simplicity and continuity among these branches, which are strongly affected and significantly destabilized by the coupling, contrast to the complicated and distant relation to the modes at low coupling. Additional simplification results from the fact that the strongly growing stationary mode is so closely related to the most strongly growing stationary SST mode in the fast-wave limit, which can be relatively easily understood (see Part III). A powerful clarity thus results from viewing the oscillatory mixed-mode branch as an extension of the strongly growing stationary mode toward lower coupling where ocean dynamics begins to regain wavelike behavior.

In this interpretation, one begins by understanding the spatial form and instability mechanisms of the mode in the fast-wave limit at moderately strong coupling. As one follows the stationary mode out to realistic values of the relative time-scale parameter, the stationary mode acquires significant oceanic time scale dependence associated with "picking up" a degree of freedom from among the low-frequency part of the scattering spectrum on the low coupling side. This amounts to giving a rigorous basis to the original interpretation of the SS and BH delayed-oscillator model, which was used to explain a coupled mode very similar to that of Figs. 17 and 18 in the Schopf and Suarez (1988) and BH intermediate models. We elaborate on this in section 6.

The fact that the standing oscillatory mixed modes connect to the scattering spectrum at low coupling for realistic values of δ suggests that the original SS and BH interpretation is actually a more faithful representation than the later models of CMZ and Schopf and Suarez (1990). The latter provide exact, rather than ad hoc, derivations but for the specialized case of coupling at a single point, in the fast-SST limit; because of the latter assumption, the low-coupling connection is to an ocean basin mode as in Fig. 13 rather than to the scattering spectrum. However, the apparent contradictions disappear when the modes are interpreted as mixed SST/ocean-dynamics modes: both approaches to the problem are just alternative approximations to the same eigensurface. This can occur because of the smooth connection of the strongly growing stationary mode from the fast-wave limit to the fast-SST limit (Fig. 11 and Fig. 13 of Part III). Both approaches are accurate (within their respective limitations) provided that the low-coupling end is ignored.

One further remark on the lack of dependence on which of the uncoupled modes goes into the mixed SST/ocean-dynamics modes: in numerical models and in the long-wave approximation, the scattering spectrum is discretized and the ocean basin modes are separated from it. For the full shallow-water equations in a meridionally unbounded basin there is simply a continuum of scattering modes and the ocean basin modes are just a less strongly scattering case (implicit in Moore 1968, chapter 4). We postulate that in this continuum case, well-defined unstable coupled modes corresponding very closely to the ones shown here will exist as quantized modes at finite coupling, whereas no quantized modes exist at zero coupling. Thus, where the oscillatory mixed branch of Figs. 15 and 16 connects to successive members of the discretized scattering spectrum in this model, the only change in the continuum case will be that the connection to the scattering spectrum will be continuous, and that no quantized modes will exist for coupling values lower than this merger. If true, this would make our argument for viewing coupled modes from the strong coupling side rigorous, rather than merely practical.

b. Relation to propagating cases

We have shown in section 3 that there are eastward- or westward-propagating SST modes in the fast-wave limit, which become unstable at sufficiently large coupling. Like the strongly growing stationary SST modes, these undergo a similar mixing with the ocean-dynamics-related modes away from the fast wave limit. Mapping out the details of the transition between a regime that oscillates purely due to propagation and one that is dominated by wave dynamics is more difficult for several reasons than mapping the transition of the previous section between a stationary SST mode and a mixed mode oscillating by wave dynamics. While 2-

degeneracies are again likely to be implicated in the connection of the eigensolution branches, if these have nonzero frequency they will be localized at isolated points somewhere in the μ–δ plane (see Appendix). For a given path between regimes, one is thus less likely to directly encounter these signposts of the transition, unlike the stationary-to-oscillation transition, for which the 2-degeneracies form curves in the μ–δ plane. There can thus be many paths in parameter space where the transition from one oscillation mechanism to another is quite smooth. Furthermore, a third parameter must be explicitly introduced into the problem, say either δ_s or ϵ_a, to move from the stationary SST mode case to the propagating case. The boundaries of the region where the leading mode is stationary form a somewhat irregular surface in this parameter space, and when tracing an eigensurface from one oscillatory regime to another, one may pass through this stationary regime or not, depending on the choice of path. In some cases the stationary regime apparently does play a fundamental role in connecting oscillatory regimes: two surfaces of oscillatory eigenvalues, which are not directly connected to each other, can each be connected to the stationary branch at separate curves of 2-degeneracy. In such cases, often the two oscillatory modes will dominate (in the sense of leading growth rate) in different domains of the parameter space, with a region of comparable growth rates in between. This raises the possibility of mode interactions (Golubitsky and Schaeffer 1985), which we are unable to pursue here (but see HNJ for a fast-wave limit case).

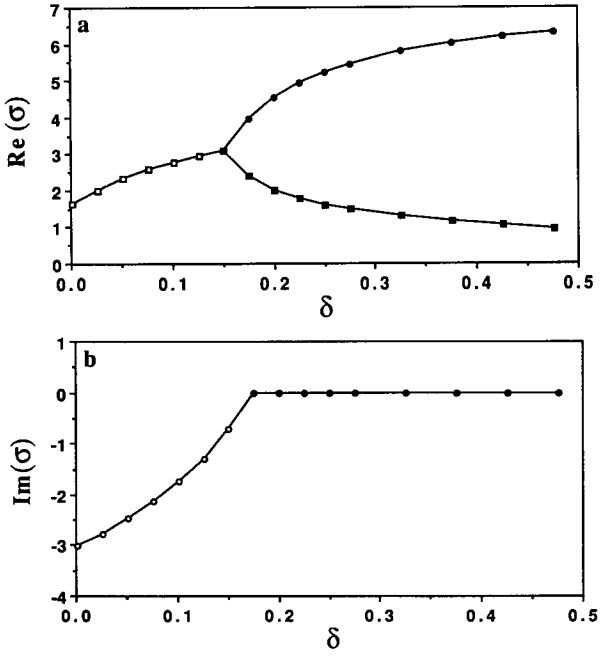

FIG. 20. Transition of an eastward-propagating SST mode to stationary modes at relatively strong coupling, for μ = 1.0, δ_s = 0, and ϵ_a = 4.0. Eigenvalues in yr^{-1} by the SST time scale.

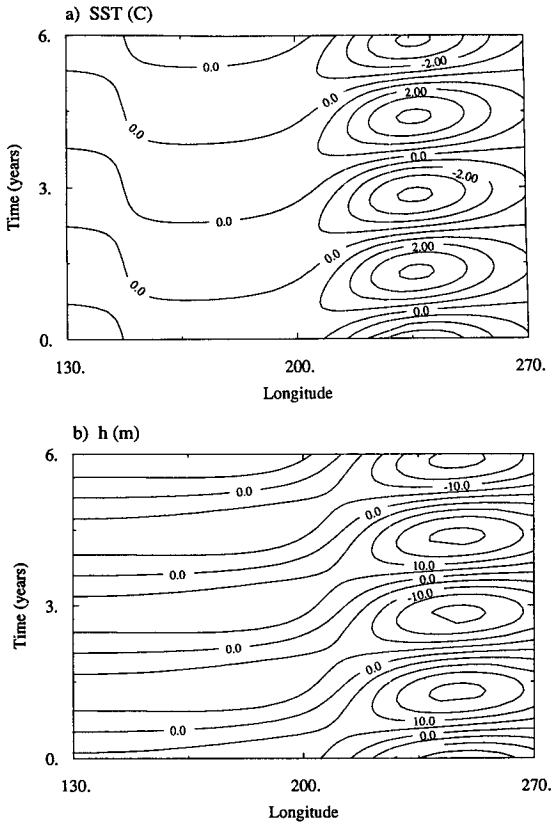

FIG. 21. As in Fig. 14 except δ = 0.25, μ = 0.8, δ_s = 0, and ϵ_a = 4.0.

We confine ourselves to two examples. Figures 20 and 21 show two cases where the SST mode at the fast-wave limit is eastward propagating, for δ_s = 0 and a value of ϵ_a which is slightly larger than standard. For the stronger coupling case (Fig. 20), tracing along a path μ = constant one quickly encounters the stationary regime and the eastward-propagating mode breaks into two real modes. The upper branch is the strongly growing stationary branch, which connects to the wave oscillation regime as before. For slightly weaker coupling, oscillation persists out to larger δ_s, but the mode smoothly loses its eastward-propagating character and takes on the form of a standing oscillation. Figure 21 shows the structure of this mode for an intermediate case, where it still retains some eastward-propagation tendency but where wave dynamics has taken on a crucial role in the oscillation.

A similar mixed mode can be also found starting from a westward-propagating SST mode as shown in Fig. 22. The transition from a pure SST mode to a mixed mode is reflected by the turning of the dependence of the eigenvalue on δ. Both growth rate and frequency decrease as δ increases away from the transition, which indicates the dependence of this oscillatory mode on the oceanic wave dynamics. The mixed nature of the mode, with westward-propagation fea-

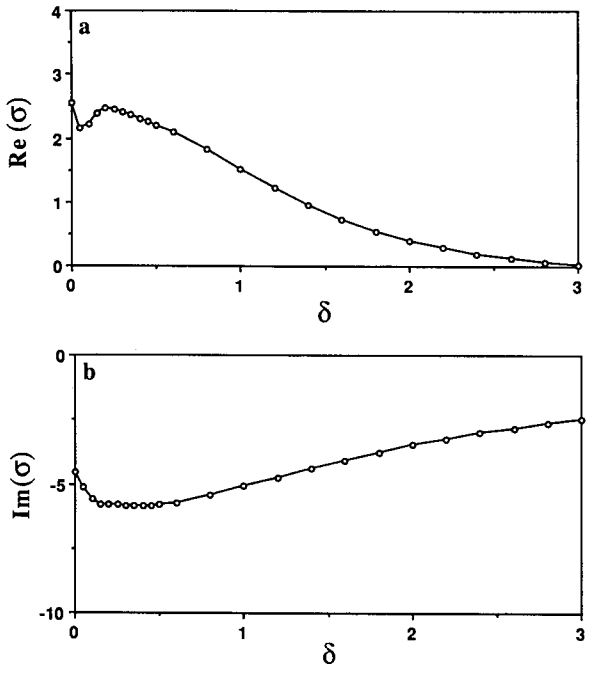

FIG. 22. As in Fig. 20 but transition of westward-propagating SST mode to a mixed SST/ocean-dynamics mode at relatively strong coupling for $\mu = 0.8$, $\delta_s = 0.6$, and $\epsilon_a = 2.0$.

tures inherited from the SST mode at the fast-wave limit and the standing oscillation appearance taken from the ocean basin modes, is demonstrated in the eigenstructure shown in Fig. 23. We note also that the transition to a stationary mode occurs at higher μ when the surface-layer feedbacks are included. While this has no effect on the qualitative relation of the flow regimes, it could be important in practical applications.

5. Nonlinear solutions

Here we do not undertake an extensive examination of nonlinear time-dependent solutions but simply show that the linear analysis is a very good indication of the finite amplitude nonlinear solutions, at least near the Hopf bifurcation. Figure 24 gives a nonlinear solution (with basic state subtracted) corresponding to the linear solution of Fig. 14. The overall structure resembles the eigenstructure with a period still around 4 years. Here the solution is far enough from the bifurcation that the amplitudes of positive and negative SST anomalies become slightly asymmetric and their positions are slightly shifted in the nonlinear solution. For the mixed mode with westward propagation of Fig. 23, a similar agreement up to small differences is found between the nonlinear solution at reasonable amplitude and the linear eigensolution shown in Fig. 25.

The parameterization of subsurface temperature in the model should be better tuned before undertaking a quantitative examination of strongly nonlinear regimes, but preliminary explorations with no surface-layer feedback are worth a brief comment. As coupling is increased, the oscillations tend to become distorted in a manner qualitatively reminiscent of the relaxation oscillations noted in HNJ, but sometimes exhibiting complicated behavior with several maxima and minima within each periodic cycle. Period-doubling behavior qualitatively like Münnich et al. (1991) is noted but appears less significant. Small regions of apparently chaotic behavior can be found but the degree of irregularity is far less than, for instance, the ZC model or observed time series. A number of additional mechanisms including seasonal cycle could potentially change this situation but have not yet been explored.

6. Discussion and conclusions

Using a stripped-down intermediate model, we examine the behavior across different parameter regimes for the leading modes of the tropical ocean–atmosphere system linearized about a climatological basic state. We undertake to show that, despite the apparent differences, there is a relatively straightforward relationship among regimes in which zonal propagation of SST, wind, current, and thermocline anomalies along the equator determine the period of the interannual oscil-

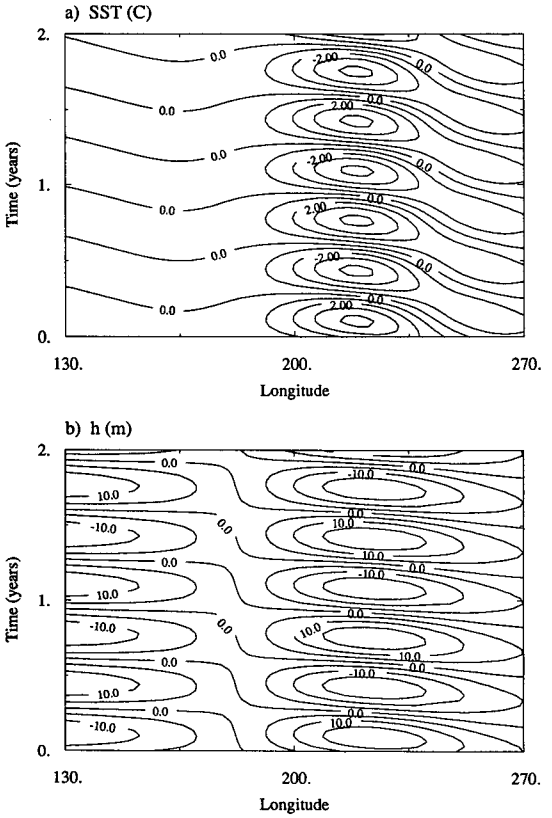

FIG. 23. As in Fig. 14 except $\delta = 1.0$, $\mu = 0.7$, $\delta_s = 0.6$, and $\epsilon_a = 2.0$.

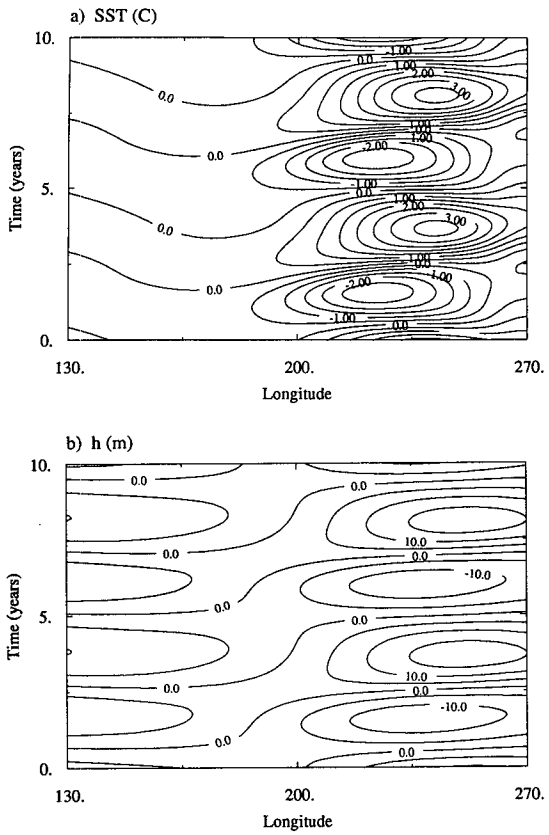

FIG. 24. Nonlinear solution corresponding to the case in Fig. 14.

lation, regimes in which the most unstable mode is purely stationary, and an important regime in which warm and cold SST anomalies alternate in the eastern basin in a standing oscillation, with subsurface ocean dynamics serving as the memory of the system. We attempt to build on and bring together previous work by several authors, by indicating how some important simple models relate to each other and to the modes of this fuller system. At the same time, we aim to show how the modes in realistic parts of parameter space are related to those in simplifying limits.

These limits and the regions of validity surrounding them are detailed in Part II and exploited to produce analytic results in Parts II and III. Here we refer to the uncoupled case, and to the fast-wave limit and the fast-SST limit, which obtain, respectively, when the time scales of wave adjustment are much faster than the time scales of SST change and vice versa. In terms of the scalar parameter, δ, defined to measure the ratio of these time scales, the fast-wave and fast-SST limits occur at small and large δ, respectively. The scalar parameter defined for coupling, μ, measures the amount of wind-stress feedback from the atmosphere per degree of SST anomaly, with $\mu = 0$ being uncoupled and $\mu = O(1)$ for moderately strong coupling. The fast-SST limit produces no real simplifications but is useful for reference to the models of CMZ and Schopf and Suarez (1990). In the fast-wave limit, the slow modes are referred to as SST modes because they are associated with the time derivative of the SST equation. These SST modes are very robust at moderate and strong coupling; they can be thought of as fundamentally coupled modes in the sense that even a modest amount of coupling alters them strongly relative to their trivially decaying uncoupled counterparts, as indicated here and examined in Part II. In the uncoupled case, the eigenmodes associated with the time derivatives of the subsurface ocean dynamics (ocean-dynamics modes) in a zonally bounded basin are of two types: the ocean basin modes of Cane and Moore (1981) and a previously overlooked class of scattering modes. At low frequencies and basin scales these are very different from the Rossby and Kelvin modes of the infinite-basin case.

As one moves from uncoupled to realistically coupled cases and from the fast-wave limit to realistic relative time-scale ratios, these ingredients will become mixed; we use the descriptive term *mixed SST/ocean-dynamics modes* to refer to modes in regimes where they are significantly modified relative to these simple limits. To show how this mixing occurs, we trace surfaces of eigenvalues that are continuously connected in parameter space. Eigensurfaces corresponding to dif-

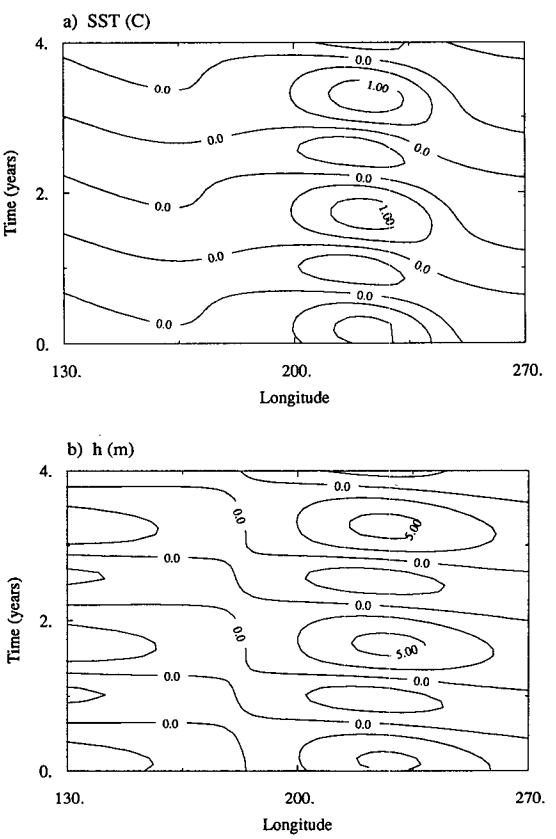

FIG. 25. Nonlinear solution corresponding to the case in Fig. 23.

ferent modes that are distinct in some regions can merge through degeneracies at which the eigenvalue and eigenstructure become identical for two or more modes. Degeneracies of multiplicity two (2-degeneracies) involving the transition between a complex conjugate pair of modes and two pure real modes are the most commonly encountered in this system. These occur as surfaces of dimension $(k-1)$ in a parameter space of dimension k, forming boundaries between a stationary regime and various oscillatory regimes in which different physical mechanisms dominate.

The relationship between flow regimes is most easily narrated by beginning from the fast-wave limit where ocean time scales are, by definition, not important and where the picture is relatively simple. Oscillation can occur by zonal propagation of anomalies: westward- or eastward-propagating regimes occur when the parameters favor different mechanisms that give these tendencies: for example, westward for large surface-layer feedbacks, eastward when surface-layer feedbacks are small and the atmospheric model damping length is short (we use "surface-layer feedbacks" to denote mechanisms due to the component of surface currents and upwelling produced by the embedded surface layer). The mechanisms are essentially those of the periodic-basin case and are discussed in the context of finite-basin effects such as quantization in Part III and HNJ.

Between these propagating regimes lies a stationary regime where the leading SST mode is purely growing and leads to multiple stationary states in the nonlinear case (see HNJ). The SST patterns resemble those that occur at the mature warm or cold phases of ENSO, extending across most of the central and eastern basin. This east basin trapping results partly from the zonal dependence of the upwelling and thermocline slope in the climatology, but has an important contribution from the β effect in atmospheric and oceanic steady-state dynamics, as analyzed in Part III. Because these features carry over into neighboring oscillatory regimes, this stationary regime in the fast-wave limit provides an excellent starting point for understanding ENSO dynamics. For the leading mode, this stationary regime extends without qualitative change for a range of surface-layer feedback strength from intermediate to zero, so we use the case without surface-layer feedbacks for much of the exploration into the role of wave dynamics.

Following the eigensurface associated with this stationary mode to larger δ, away from the fast-wave limit, one finds that for coupling values stronger than a certain threshold, where this stationary mode stands out as more strongly growing than other modes, the eigensurface extends without substantial change from the fast-wave limit all the way to the fast-SST limit. An analysis of why this must occur at strong coupling is given in Part III; essentially, coupling time scales become faster than those associated with ocean dynamics, so ocean wave propagation in the conventional sense becomes secondary. This is pivotal in understanding the coupled system because 1) it allows the spatial form and growth mechanisms of important coupled regimes to be understood from the fast-wave limit and 2) it implies that modes associated with ocean dynamics must connect somehow to this strongly growing mode.

At lower coupling, this indeed happens as the strongly growing stationary mode connects, via a curve of 2-degeneracy in the μ–δ parameter plane, to an oscillatory eigensurface. The oscillatory regime just to the lower coupling side of this 2-degeneracy is an important one for models such as the ZC model and the SS intermediate model, and presumably for the observed system. It has a standing oscillation in SST, with a spatial form extremely similar to the stationary SST mode, and is destabilized by the same coupling mechanisms. The memory for the oscillation is provided by subsurface oceanic dynamics, characterized by deepening of the thermocline in the western basin prior to the deepening in the east. This regime extends across a considerable range of δ, from the fast-SST limit to $\delta = O(1)$. It terminates in a 3-degeneracy where the 2-degeneracy curve just mentioned meets another such curve, completing the connection to the low-coupling stationary branch of the SST mode.

The description becomes temporarily complicated when one attempts to describe the connection of this standing oscillation regime to the uncoupled case. At lower μ, this oscillatory eigensurface connects not to a single mode from the uncoupled oceanic dynamics spectrum but to a series of them: beginning from $\delta = O(1)$ where the standing oscillation first arises, the low-coupling end of the branch attaches first to the lowest-frequency mode of the scattering spectrum, then to sequentially higher-frequency scattering modes, and finally to the gravest ocean basin mode in the region approaching the fast-SST limit. These successive connections are accomplished by a sequence of 2-degeneracies, each of which has complex eigenvalue and thus occurs at a point in the μ–δ plane (see Appendix), that interlink the branches arising from the uncoupled ocean as they become destabilized relative to their uncoupled decay rate. In each case, there is a dramatic structural change between the uncoupled modes and the standing oscillation regime, while the latter is almost completely insensitive to what happens at low coupling.

A fair summary of this situation is that the standing oscillation does not care which uncoupled ocean mode it is attached to; its properties are fundamentally determined by the coupling, and it is best approached conceptually from the strong coupling side. It is much simpler to view the standing-oscillation regime as an extension of the strongly growing stationary mode toward lower coupling, where ocean dynamics begins to regain some aspects of wavelike behavior. In this interpretation, one begins by understanding the spatial form and instability mechanisms of the mode in the fast-wave limit at moderately strong coupling. As one

follows the stationary mode out to realistic values of the relative time-scale parameter, the stationary mode acquires significant oceanic time-scale dependence associated with "picking up" a degree of freedom from among the low-frequency part of the scattering spectrum on the low coupling side.

This view is remarkably consistent, in terms of physical content, with the original interpretation of the SS and BH delayed-oscillator "toy" model, since this is based on the SST equation for a small eastern basin box, with a delay term representing the time scales of ocean adjustment. Both SS and BH used the delayed-oscillator model to explain a mode found in their respective intermediate models that is essentially the same as the standing-oscillation regime discussed here. The toy model SST equation gives pure growth (by assumption) in the fast-wave limit, and a surface of 2-degeneracy gives the transition to oscillation as wave time scales become important. As long as the oscillatory regime is approached from the high-coupling side, and provided the wave delay term is interpreted as a perturbation by wave dynamics in the broader sense rather than in terms of a single Rossby and Kelvin wave, there is a very good qualitative match to the leading mode of the fuller coupled system examined here.

Because the standing-oscillatory mixed modes connect to the scattering spectrum at low coupling (for realistic values of the relative time scale coefficient), our results suggest that the original SS and BH interpretation is, in fact, a slightly more faithful representation than the later models of CMZ and Schopf and Suarez (1990). The latter are derived more rigorously but are formulated in the fast-SST limit where the low-coupling connection is to an ocean basin mode. However, because of the smooth connection of the strongly growing stationary mode from the fast-wave limit to the fast-SST limit and the resulting smooth connection of the standing-oscillatory regime across a large range of parameters, these seemingly contradictory approaches to the problem are just alternative approximations to the same eigensurface. Both are accurate provided that the low-coupling end is ignored. In other words, coupling plays such a decisive role in determining period, stability, and spatial structure that conventional uncoupled ocean wave dynamics is largely irrelevant, and the apparent contradictions between these models disappear when interpreted as mixed SST/ocean-dynamics modes.

From the standing-oscillation regime, it is easy to move smoothly and gradually to a regime of the mixed SST/ocean-dynamics modes where propagation occurs during parts of the cycle and contributes to the period to some extent. Such a regime is probably the best analog to the observed system. The details of how the various surfaces of eigenvalues are connected over the full range of parameters are more subtle to unravel in this case than in the transition between the stationary and standing-oscillation regimes because at least a third parameter is involved (e.g., the surface-layer coefficient). However, the basic point that these characteristics can coexist within the same mixed mode is easily understood. The standing-oscillation regime provides one simple case that emphasizes the role of subsurface dynamics in determining periodicity; the fast-wave-limit propagating cases provide alternate simple cases in which periodicity is provided by zonal phase lags. Since these are all continuously connected, regimes with some properties of each arise in between. There is thus no contradiction between evidence for involvement of subsurface dynamics in the ENSO cycle (e.g., Latif et al. 1993; Latif and Graham 1992; Graham and White 1990) and indications of other contributing mechanisms (e.g., Barnett et al. 1991).

Integrations of the nonlinear model verify that, for the Hopf bifurcations studied here, the linear eigenmodes indeed provide a good approximation to the spatial form and period of the nonlinear cycles out to physically realistic amplitudes. Stationary bifurcations will be identical to those found in the fast-wave limit (since all time derivatives are zero), examples of which are given in HNJ.

While far from exhausting the study of the bifurcation diagram of the tropical coupled system, the aspects studied here cover the predominant range of behaviors noted in coupled models of intermediate, hybrid, and GCM classes in the hierarchy, at least for the primary bifurcation from the climate state. It is of course possible to choose many other parameters to move between the same behavior regimes: for instance, Wakata and Sarachik (1991) use width of the equatorial upwelling region as a parameter to move between the standing-oscillation regime and the eastward-propagating regime (in a version close to Hirst 1988); Wakata and Sarachik, BH, and CMZ all encounter the 2-degeneracy separating the standing-oscillation regime from the stationary growth regime. In Fig. 11 of BH, for instance, this 2-degeneracy surface is crossed by changing the SST damping rate, which is roughly equivalent to a small change in coupling (accompanied by a small change in δ, in our terminology), that is, a small section from the center of our Fig. 15 or 16. While the BH intermediate model formulation and parameters are very closely related to ours, small differences—such as details of the thermocline feedback formulation—make it difficult to calculate the exact mapping of their parameter space onto ours. What is important is the topological equivalence of the structures of the eigensurfaces. Adding or modifying feedback mechanisms will also shift the regime boundaries: for example, inclusion of surface-layer feedbacks moves the stationary-regime transition to higher coupling than when thermocline feedback alone is active in our model. While this can be important to quantitative work, the qualitative aspects remain the same over

substantial parameter ranges. The parameter set selected here suffices to capture the essential connections between behavior regimes in a concise manner.

Given that the most physically realistic part of parameter space is transected by a number of higher-codimension bifurcations (including double-zero eigenvalue bifurcations corresponding to the main surfaces of 2-degeneracy emphasized here) that separate it into regions of qualitatively different behavior, it is not surprising that the coupled system exhibits great sensitivity. In the coupled GCM intercomparison of Neelin et al. (1992), interannual variability of both zonally propagating and standing-oscillation types was noted in the SST simulations of different models, while some had climate drift that appeared to involve coupled feedbacks of a similar nature and multiple stationary states were noted in some hybrid models. Both propagating and standing types of SST variability had aspects that resembled the ENSO phenomenon, although criteria for sufficient resemblance to count as ENSO-like did engender some lively discussion among the respective modeling groups.

If one broadens the term "parameter space" to more loosely include the many differences in formulation of parameterized processes, model resolution, etc., we would argue that there are close parallels between the GCM behavior and the parameter-space dependence demonstrated here. In particular, that it is possible to move continuously on the eigensurface for the most unstable mode from a propagating regime to a stationary regime to a standing-oscillatory regime suggests that the qualitative resemblance among some propagating and standing oscillations in the GCMs is far from accidental. They can be thought of as, in some sense, the same mode in different regimes of behavior (provided that only the first bifurcation is involved). It is very possible for them to share similar physical mechanisms contributing to their growth and spatial structure, even if the oscillation mechanisms differ. In creating coupled GCMs from oceanic and atmospheric models tested as components individual components, it is difficult to know a priori into which regime the combination will fall in the coupled parameter space. We hope that the analysis presented here will at least provide a conceptual framework for discussing the results.

Acknowledgments. This work was supported by National Science Foundation Grants ATM-9215090 (JDN and FFJ) and ATM-9013217 (FFJ) and by National Oceanographic and Atmospheric Administration Grant NA16RC0178-01 (FFJ and JDN; the views expressed are those of the authors and do not necessarily reflect those of NOAA). Part of the computation was carried out at the San Diego Supercomputing Center and at the National Center for Atmospheric Research. The authors thank W. Weibel for greatly improving some of the figures and P.-O. Nallet for the explorations of highly nonlinear regimes mentioned in the last paragraph of section 5. We are particularly indebted to Z. Hao, J.-D. Li, and J. Zhao for careful comments on the numerical scheme. C. Wong typeset the manuscript. We acknowledge enjoyable discussions with many colleagues, including D. Battisti, T. Barnett, M. Cane, P. Gent, H. Dijkstra, I. Held, A. Hirst, M. Latif, D. Moore, G. Philander, E. Sarachik, and P. Schopf. Both authors thank M. Ghil for unfaltering encouragement. An earlier version of this work appeared in the *Proceedings of the Eighth Conference on Atmospheric and Oceanic Waves and Stability*, sponsored by the American Meteorological Society in 1991.

APPENDIX

Degeneracies

To provide qualitative insight into the form of the dispersion diagrams in the vicinity of degeneracies (as seen in Figs. 13a,b; 15a,b; 16a,b), consider a dispersion relation

$$F(\sigma, \mu) = 0, \tag{A.1}$$

where σ is the eigenvalue, μ a vector of parameters, and F a smooth scalar function such that

$$(F(\sigma))^* = F(\sigma^*). \tag{A.2}$$

In our case F is a polynomial of order $N \sim 400$, since $F = \det[\sigma I - Df(\bar{x}, \mu)]$ for a system $\dot{x} = f(x, \mu)$, $x \in \mathbf{R}^N$, linearized about a fixed point $\bar{x}$, with $Df = [\partial f_i/\partial x_j]$, for a smooth vector function $f : \mathbf{R}^N \to \mathbf{R}^N$.

Expanding F in a Taylor series about a solution $(\bar{\sigma}, \bar{\mu})$, where $\partial F/\partial \sigma \neq 0$, leads to

$$\sigma' = -\left(\frac{\partial F}{\partial \sigma}\right)^{-1} \frac{\partial F}{\partial \mu} \mu' + O(\sigma'^2, \mu'^2), \tag{A.3}$$

where (σ', μ') denotes departures from $(\bar{\sigma}, \bar{\mu})$ and $\partial F/\partial \mu = [\partial F/\partial \mu_i]^T$. Thus, the eigensurface has a unique continuation in parameter space about such a point [note: the form (A.1)–(A.3) is not the most useful for numerical purposes and is used here for illustration only].

The degeneracies of algebraic multiplicity two occur where

$$\partial F/\partial \sigma = 0, \tag{A.4}$$

but $\partial^2 F/\partial \sigma^2 \neq 0$. We apparently encounter only the generic behavior, which is algebraically double but geometrically simple with only one eigenvector associated with the double eigenvalue; in principle, we could construct a generalized eigenvector to complete the eigenspace (Iooss and Joseph 1990). In the vicinity of a solution $(\bar{\sigma}, \bar{\mu})$ where an algebraically double degeneracy occurs

$$\sigma'^2 = \left(\frac{\partial^2 F}{\partial \sigma^2}\right)^{-1} \frac{\partial F}{\partial \mu} \mu' + O(\sigma'^3, \mu'^2) \tag{A.5}$$

so two eigensurfaces merge in a manner that locally has a square root dependence on μ'. In the figures, a single parameter μ_i is varied so

$$\sigma' = \pm b\mu_i^{1/2}, \tag{A.6}$$

where $b = [(\partial^2 F/\partial\sigma^2)^{-1}\partial F/\partial\mu_i]^{1/2}$ is potentially complex; occasional apparent departures in the figures from the $\mu_i^{1/2}$ dependence are due to insufficient resolution in the plotting routine. For the case of a 2-degeneracy with $\bar{\sigma}$ pure real (which implies $\partial^2 F/\partial\sigma^2$ and $\partial F/\partial\mu$ pure real), σ' is thus pure real on one side of the 2-degeneracy and pure imaginary on the other.

Why this is by far the most common case in the figures becomes clear when considering, for example, for polynomial F, that the dual constraints (A.1) and (A.4)

$$F = \sum_{n=0}^{N} a_n\sigma^n = 0 \tag{A.7}$$

$$\frac{\partial F}{\partial\sigma} = \sum_{n=1}^{N} n a_n\sigma^{n-1} = 0 \tag{A.8}$$

imply a relationship among the parameters that is a surface of lower dimension in a k dimensional parameter space. Consider σ to be given by (A.8). For σ real (A.7) can be solved for a relation among the coefficients $\{a_n(\mu)\}$, which (assuming suitably smooth dependence on the control parameters) implicitly gives a surface of dimension $k - 1$. For complex σ, the additional constraint that a_n are real leads to a surface of lower dimension $k - 2$. For a two-parameter slice such as presented in section 4, 2-degeneracies with σ real occur as curves, while those with complex σ occur at isolated points. In the one-parameter slices as a function of coupling in Figs. 13, 15, and 16, the 2-degeneracy separating the standing-oscillatory region from the stationary region is thus always encountered, while the complex 2-degeneracies are not seen in a typical slice, although they are essential to the connection to different modes from the uncoupled ocean spectrum. The 3-degeneracy with σ real in section 4, given by the additional condition $\partial^2 F/\partial\sigma^2 = 0$, also has dimension $k - 2$.

The leading eigensurfaces traced in sections 3 and 4 correspond to the primary bifurcation of the original system for some set of parameter values wherever $\mathrm{Re}(\sigma)$ exceeds the physical damping times of the system, since the damping parameters can shift a given point on the surface to meet the condition $\mathrm{Re}(\sigma) = 0$. The 2-degeneracy marking the transition from the stationary to standing-oscillatory mode is then a codimension-two bifurcation (double-zero eigenvalue) according to the number of parameters required to obtain the bifurcation in a persistent way (e.g., Guckenheimer and Holmes 1983), while the 3-degeneracy is a codimension-3 bifurcation. The complex 2-degeneracies involved in the transition between connections to the ocean scattering spectrum do not meet this condition and are unlikely to correspond to higher-codimension bifurcations of the original system for any parameter range. Indications of possible codimension-two bifurcations involving two modes (imaginary pair and a zero eigenvalue, or two imaginary pairs) have been noted but not pursued.

REFERENCES

Anderson, D. L. T., and J. P. McCreary, 1985: Slowly propagating disturbances in a coupled ocean–atmosphere model. *J. Atmos. Sci.*, **42**, 615–629.

Barnett, T. P., N. Graham, M. Cane, S. Zebiak, S. Dolan, J. O'Brien, and D. Legler, 1988: On the prediction of El Niño of 1986–1987. *Science*, **241**, 192–196.

——, M. Latif, E. Kirk, and E. Roeckner, 1991: On ENSO physics. *J. Climate*, **4**, 487–515.

Battisti, D. S., 1988: The dynamics and thermodynamics of a warming event in a coupled tropical atmosphere–ocean model. *J. Atmos. Sci.*, **45**, 2889–2919.

——, 1989: On the role of off-equatorial oceanic Rossby waves during ENSO. *J. Phys. Oceanogr.*, **19**, 551–559.

——, and Hirst, A. C., 1989: Interannual variability in the tropical atmosphere/ocean system: Influence of the basic state and ocean geometry. *J. Atmos. Sci.*, **46**, 1687–1712.

Bjerknes, J., 1969: Atmospheric teleconnections from the equatorial Pacific. *Mon. Wea. Rev.*, **97**, 163–172.

Cane, M. A., 1979a: The response of an equatorial ocean to simple wind stress patterns: I. Model formulation and analytic results. *J. Mar. Res.*, **37**, 233–252.

——, 1979b: The response of an equatorial ocean to simple wind stress patterns: II. Numerical results. *J. Mar. Res.*, **37**, 253–299.

——, and E. S. Sarachik, 1977: Forced baroclinic ocean motions: II. The linear equatorial bounded case. *J. Mar. Res.*, **35**, 395–432.

——, and D. W. Moore, 1981: A note on low-frequency equatorial basin modes. *J. Phys. Oceanogr.*, **11**, 1578–1584.

——, and E. S. Sarachik, 1981: The response of a linear baroclinic equatorial ocean to periodic forcing. *J. Mar. Res.*, **39**, 651–693.

——, and S. E. Zebiak, 1985: A theory for El Niño and the Southern Oscillation. *Science*, **228**, 1084–1087.

——, S. E. Zebiak, and S. C. Dolan, 1986: Experimental forecasts of El Niño. *Nature*, **321**, 827–832.

——, M. Münnich, and S. E. Zebiak, 1990: A study of self-excited oscillations of the tropical ocean–atmosphere system. Part I: Linear analysis. *J. Atmos. Sci.*, **47**, 1562–1577.

Chao, Y., and S. G. H. Philander, 1993: On the structure of the Southern Oscillation. *J. Climate*, **6**, 450–469.

Ghil, M., M. Kimoto, and J. D. Neelin, 1991: Nonlinear dynamics and predictability in the atmospheric sciences. *Rev. Geophys.* (Suppl.), 46–55, U.S. Natl. Rep. to the Int. Union Geod. Geophys. 1987–1990.

Gill, A. E., 1980: Some simple solutions for heat induced tropical circulation. *Quart. J. Roy. Meteor. Soc.*, **106**, 447–462.

——, 1985: Elements of coupled ocean–atmosphere models for the tropics. *Coupled Ocean–Atmosphere Models, Elsevier Oceanogr. Ser.*, **40**.

——, and A. J. Clarke, 1974: Wind-induced upwelling, coastal current, and sea-level changes. *Deep-Sea Res.*, **21**, 325–345.

——, and E. M. Rasmusson, 1983: The 1982–1983 climate anomaly in the equatorial Pacific. *Nature*, **306**, 229–234.

Golubitsky, M., and Schaeffer, 1985: *Singularities and Groups in Bifurcation Theory, Vol.* 1. Springer-Verlag, 463 pp.

——, I. Stewart, and D. G. Schaeffer, 1988: *Singularities and Groups in Bifurcation Theory, Vol.* 2. Springer-Verlag, 533 pp.

Gordon, C., 1989: Tropical ocean–atmosphere interactions in a coupled model. *Phil. Trans. Roy. Soc. London*, **A329**, 207–223.

Graham, N. E., and W. B. White, 1988: The El Niño cycle: Pacific ocean-atmosphere system. *Science,* **240,** 1293–1302.

——, and ——, 1990: The role of the western boundary in the ENSO cycle: Experiments with coupled models. *J. Phys. Oceanogr.,* **20,** 1935–1948.

Guckenheimer, J., and P. Holmes, 1983: *Nonlinear Oscillations, Dynamical Systems, and Bifurcations of Vector Fields.* Applied Mathematical Sciences 42, F. John, J. E. Marsden, and L. Sirovich, Eds., Springer-Verlag, 454 pp.

Hao, Z., J. D. Neelin, and F.-F. Jin, 1993: Nonlinear tropical air–sea interaction in the fast-wave limit. *J. Climate,* **6,** 1523–1544.

Hirst, A. C., 1986: Unstable and damped equatorial modes in simple coupled ocean-atmosphere models. *J. Atmos. Sci.,* **43,** 606–630.

——, 1988: Slow instabilities in tropical ocean basin-global atmosphere models. *J. Atmos. Sci.,* **45,** 830–852.

Iooss, G., and D. D. Joseph, 1990: *Elementary Stability and Bifurcation Theory.* Springer-Verlag, 324 pp.

Jin, F.-F., and J. D. Neelin, 1993: Modes of interannual tropical ocean-atmosphere interaction—A unified view. Part III: Analytical results in fully coupled cases. *J. Atmos. Sci.,* **50,** 3523–3540.

Latif, M., and A. Villwock, 1990: Interannual variability as simulated in coupled ocean–atmosphere models. *J. Mar. Systems,* **1,** 51–60.

——, and N. E. Graham, 1992: How much predictive skill is contained in the thermal structure of an OGCM? *J. Phys. Oceanogr.,* **22,** 951–962.

——, A. Sterl, E. Maier-Reimer, and M. M. Junge, 1993: Structure and predictability of the El Niño/Southern Oscillation phenomenon in a coupled ocean–atmosphere general circulation model. *J. Climate,* **6,** 700–708.

Lau, K. M., 1981: Oscillations in a simple equatorial climate system. *J. Atmos. Sci.,* **38,** 248–261.

Lau, N. C., S. G. H. Philander, and M. J. Nath, 1992: Simulation of El Niño/Southern Oscillation phenomena with a low-resolution coupled general circulation model of the global ocean and atmosphere. *J. Climate,* **5,** 284–307.

Lindzen, R. S., and S. Nigam, 1987: On the role of sea surface temperature gradients in forcing low level winds and convergence in the tropics. *J. Atmos. Sci.,* **44,** 2440–2458.

McCreary, J. P., 1976: Eastern tropical ocean response to changing wind systems with application to El Niño. *J. Phys. Oceanogr.,* **6,** 632–645.

Matsuno, T., 1966: Quasi-geostrophic motions in the equatorial area. *J. Meteor. Soc. Japan,* Ser. II, **44,** 25–43.

Mechoso, C. R., C.-C. Ma, J. D. Farrara, J. Spahr, and R. W. Moore, 1993: Parallelization and distribution of a coupled atmosphere–ocean general circulation model. *Mon. Wea. Rev.,* **121,** 2062–2076.

Meehl, G. A., 1990a: Seasonal cycle forcing of El Niño–Southern Oscillation in a global coupled ocean–atmosphere GCM. *J. Climate,* **3,** 72–98.

——, 1990b: Development of global coupled ocean–atmosphere general circulation models. *Climate Dyn.,* **5,** 19–33.

Moore, D. W., 1968: Planetary-gravity waves in an equatorial ocean. Ph.D. thesis, Harvard University, Cambridge, MA, 207 pp.

Münnich, M., M. A. Cane, and S. E. Zebiak, 1991: A study of self-excited oscillations in a tropical ocean-atmosphere system. Part II: Nonlinear cases. *J. Atmos. Sci.,* **48,** 1238–1248.

Nagai, T., T. Tokioka, M. Endoh, and Y. Kitamura, 1992: El Niño-Southern Oscillation simulated in an MRI atmosphere-ocean coupled general circulation model. *J. Climate,* **5,** 1202–1233.

Neelin, J. D., 1988: A simple model for surface stress and low level flow in the tropical atmosphere driven by prescribed heating. *Quart. J. Roy. Meteor. Soc.,* **114,** 747–770.

——, 1989a: A note on the interpretation of the Gill model. *J. Atmos. Sci.,* **46,** 2466–2468.

——, 1989b: Interannual oscillations in an ocean general circulation model coupled to a simple atmosphere model. *Phil. Trans. Roy. Soc. London,* **329A,** 189–205.

——, 1990: A hybrid coupled general circulation model for El Niño studies. *J. Atmos. Sci.,* **47,** 674–693.

——, 1991: The slow sea surface temperature mode and the fast-wave limit: Analytic theory for tropical interannual oscillations and experiments in a hybrid coupled model. *J. Atmos. Sci.,* **48,** 584–606.

——, and I. M. Held, 1987: Modelling tropical convergence based on the moist static energy budget. *Mon. Wea. Rev.,* **115,** 3–12.

——, and F.-F. Jin, 1993: Modes of interannual tropical ocean–atmosphere interaction—A unified view. Part II: Analytical results in the weak-coupling limit. *J. Atmos. Sci.,* **50,** in press.

——, M. Latif, M. A. F. Allaart, M. A. Cane, U. Cubasch, W. L. Gates, P. R. Gent, M. Ghil, C. Gordon, N. C. Lau, C. R. Mechoso, G. A. Meehl, J. M. Oberhuber, S. G. H. Philander, P. S. Schopf, K. R. Sperber, A. Sterl, T. Tokioka, J. Tribbia, and S. E. Zebiak, 1992: Tropical air–sea interaction in general circulation models. *Climate Dyn.,* **7,** 73–104.

Philander, S. G. H., 1981: The response of the equatorial oceans to a relaxation of the trade winds. *J. Phys. Oceanogr.,* **11,** 176–189.

——, and R. C. Pacanowski, 1980: The generation of equatorial currents. *J. Geophys. Res.,* **85,** 1123–1136.

——, T. Yamagata, and R. C. Pacanowski, 1984: Unstable air–sea interactions in the tropics. *J. Atmos. Sci.,* **41,** 604–613.

——, R. C. Pacanowski, N. C. Lau, and M. J. Nath, 1992: A simulation of the Southern Oscillation with a global atmospheric GCM coupled to a high-resolution, tropical Pacific Ocean GCM. *J. Climate,* **5,** 308–329.

Rasmusson, E. M., and T. H. Carpenter, 1982: Variations in tropical sea surface temperature and surface wind fields associated with the Southern Oscillation/El Niño. *Mon. Wea. Rev.,* **110,** 354–384.

Schopf, P. S., and M. A. Cane, 1983: On equatorial dynamics, mixed layer physics and sea surface temperature. *J. Phys. Oceanogr.,* **13,** 917–935.

——, and M. J. Suarez, 1988: Vacillations in a coupled ocean–atmosphere model. *J. Atmos. Sci.,* **45,** 549–566.

——, and ——, 1990: Ocean wave dynamics and the time scale of ENSO. *J. Phys. Oceanogr.,* **20,** 629–645.

Sperber, K. R., S. Hameed, 1991: Southern Oscillation in the OSU coupled upper ocean-atmosphere GCM. *Climate Dyn.,* **6,** 83–97.

Suarez, M. J., and P. S. Schopf, 1988: A delayed action oscillator for ENSO. *J. Atmos. Sci.,* **45,** 3283–3287.

Wakata, Y., and E. S. Sarachik, 1991: Unstable coupled atmosphere–ocean basin modes in the presence of a spatially varying basic state. *J. Atmos. Sci.,* **48,** 2060–2077.

Yamagata, T., 1985: Stability of a simple air–sea coupled model in the tropics. *Coupled Ocean–Atmosphere Models, Elsevier Oceanogr. Ser.,* **40,** 637–658.

——, and Y. Masumoto, 1989: A simple ocean–atmosphere coupled model for the origin of warm El Niño Southern Oscillation event. *Phil. Trans. Roy. Soc. London,* **A329,** 225–236.

Zebiak, S. E., 1986: Atmospheric convergence feedback in a simple model for El Niño. *Mon. Wea. Rev.,* **114,** 1263–1271.

——, and M. A. Cane, 1987: A model El Niño–Southern Oscillation. *Mon. Wea. Rev.,* **115,** 2262–2278.